INTERNATIONAL STUDIES IN THE FIELD OF

ELECTRICAL ELECTRONICS AND COMMUNICATION ENGINEERING

EDITOR

Doç Dr. Yelda KARATEPE MUMCU

DECEMBER 2025

DECEMBER 2025

gece kitaplığı

İmtiyaz Sahibi / Yaşar Hız
Yayına Hazırlayan / Gece Kitaplığı

Birinci Basım / Aralık 2025 - Ankara
ISBN / 978-625-8570-53-3

Gece Kitaplığı
Kızılay Mah. Fevzi Çakmak 1. Sokak
Ümit Apt No: 22/A Çankaya/ANKARA
0312 384 80 40
www.gecekitapligi.com / gecekitapligi@gmail.com

Baskı & Cilt
Bizim Büro
Sertifika No: 42488

INTERNATIONAL STUDIES IN THE FIELD OF ELECTRICAL ELECTRONICS AND COMMUNICATION ENGINEERING

ARALIK 2025

EDITOR

Doç Dr. Yelda KARATEPE MUMCU

gece kitaplığı

CONTENTS

CHAPTER 1

SEMANTIC SEGMENTATION: FUNDAMENTALS, DEEP LEARNING ARCHITECTURES, AND APPLICATIONS

Selami PARMAKSIZOĞLU[1]

1 Assistant Prof. Dr., Antalya Bilim University, School of Civil Aviation, Department of Pilotage, Antalya, Türkiye, salami.parmaksizoglu@antalya.edu.tr, https://orcid.org/0009-0001-2763-4156

1. Introduction

Semantic segmentation is the task of classifying each pixel in an image into specific categories, segmenting the image into parts that can be interpreted as different objects or regions. This process can be conceptualized through a linguistic analogy: just as a sentence derives meaning from the arrangement of individual words, semantic segmentation constructs a comprehensive visual interpretation by assigning a specific semantic class label to each constituent pixel, thereby generating a structured understanding of the scene. This process allows a machine to recognize various elements within an image and understand their spatial relationships and context.

The importance of semantic segmentation is evident in applications such as autonomous driving and medical imaging. In autonomous driving, correctly identifying objects like pedestrians, other vehicles, and lane markings is crucial for safe navigation. For instance, a self-driving vehicle depends on high-precision segmentation to distinguish critical entities, such as a child crossing the street, from static background elements like the roadside. This differentiation is fundamental to the system's ability to respond effectively within dynamic environments (Liu & Yang, 2023). Similarly, in medical imaging, semantic segmentation plays a pivotal role in diagnosing conditions by enabling detailed analysis of various tissues within images, such as the segmentation of MRI scans, which facilitates the accurate differentiation between healthy brain tissue and tumors (Sun et al., 2021).

The semantic segmentation paradigm has undergone a fundamental transformation with the advent of deep learning, most notably through Fully Convolutional Networks (FCNs). While classical methods depended on handcrafted features that often failed to capture complex spatial variances, FCNs introduced an end-to-end learning capability. This shift allowed models to automatically extract hierarchical features directly from raw data, preserving spatial resolution more effectively than traditional approaches. This transition enabled advancements in accuracy and efficiency, as seen in models such as U-Net, which have become synonymous with high-performance segmentation tasks in medical imaging (Kong et al., 2024). Recent innovations continue to enhance these capabilities further, illustrating the robustness of semantic segmentation methods in processing complex images.

This chapter first outlines the fundamental principles of semantic segmentation, detailing its methodology and historical context. Subsequently, it examines notable algorithms and architectures, with a specific focus on the impact of deep learning. Finally, the chapter discusses future trends and challenges, exploring how advancements such as transfer learning and weakly supervised methods are shaping the future of image analysis. Figure 1 shows a graphical abstract of this chapter.

Figure 1. Introduction to Semantic Segmentation

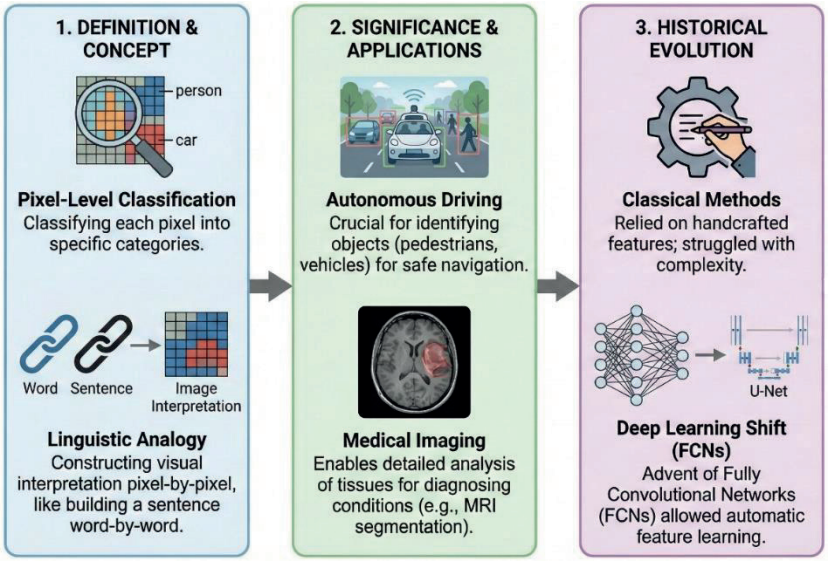

2. Comparative Analysis of Segmentation Types: Semantic, Instance, and Panoptic Approaches

Semantic segmentation, instance segmentation, and panoptic segmentation are critical tasks in computer vision, each serving unique yet interconnected purposes for understanding and interpreting visual data. These methodologies can be effectively differentiated by analyzing a complex street scene containing multiple dynamic entities (e.g., cars, pedestrians) and static infrastructure. In the context of semantic segmentation, the primary objective is pixel-level classification based solely on category. All instances of the same class share the same label, leading to a categorical output. Within the referenced scene, all pixels corresponding to the 'car' class are assigned an identical label, regardless of which specific vehicle they belong to. Consequently, while the global context is recognized, individual object instances remain indistinguishable, creating a categorical rather than distinct representation (Cheng et al., 2021).

Conversely, instance segmentation goes a step further by not only identifying the class for each pixel but also distinguishing between different instances of the same class. For the street scene, instance segmentation would identify each individual car and pedestrian separately, providing a unique label for each object. So, in a scenario with three cars and two pedestrians, the output would show each car and each pedestrian with its own distinct label, allowing for identification of individual objects within the same class (Li et al., 2018; Kirillov et al., 2019).

Panoptic segmentation synthesizes these approaches by introducing the dichotomy of 'stuff' (amorphous regions like roads and sky) and 'things' (countable objects like pedestrians and cars). This unified framework assigns a semantic label to every pixel while simultaneously generating unique identifiers for distinct instances of 'things,' thereby preserving both environmental context and individual object identities (Wang et al., 2022; Cheng et al., 2019). Table 1 shows a comparison of segmentation methods.

Table 1. Comparison of segmentation methodologies.

Segmentation Type	Goal	Output Format	Key Characteristics
Semantic Segmentation	Classify each pixel into predefined categories	Each pixel receives a class label without distinguishing instances	Does not resolve multiple instances of the same class; focuses on semantic context
Instance Segmentation	Identify and segment each object instance within an image	Each pixel of an object instance is labeled distinctly; outlines individual objects	Provides unique identification of object instances; effective for object detection
Panoptic Segmentation	Combine semantic and instance segmentation	Each pixel has both a semantic label and an instance ID, achieving a fully annotated output	Unifies recognition of background (stuff) and objects (things); more complete scene understanding

Through these tasks, the combined capabilities of semantic, instance, and panoptic segmentation contribute significantly to various applications, including autonomous driving and robotics, where understanding the environment is crucial. Each methodology offers distinct advantages tailored to specific operational requirements. In conclusion, semantic, instance, and panoptic segmentation represent interrelated strategies that, when selected appropriately, enable a robust and comprehensive understanding of visual data. Their combined insights facilitate advancements across various fields, from autonomous navigation systems to detailed scene analysis in medical imaging and beyond. Figure 2 shows a comparative analysis of segmentation types.

Figure 2. Comparative analysis of segmentation types.

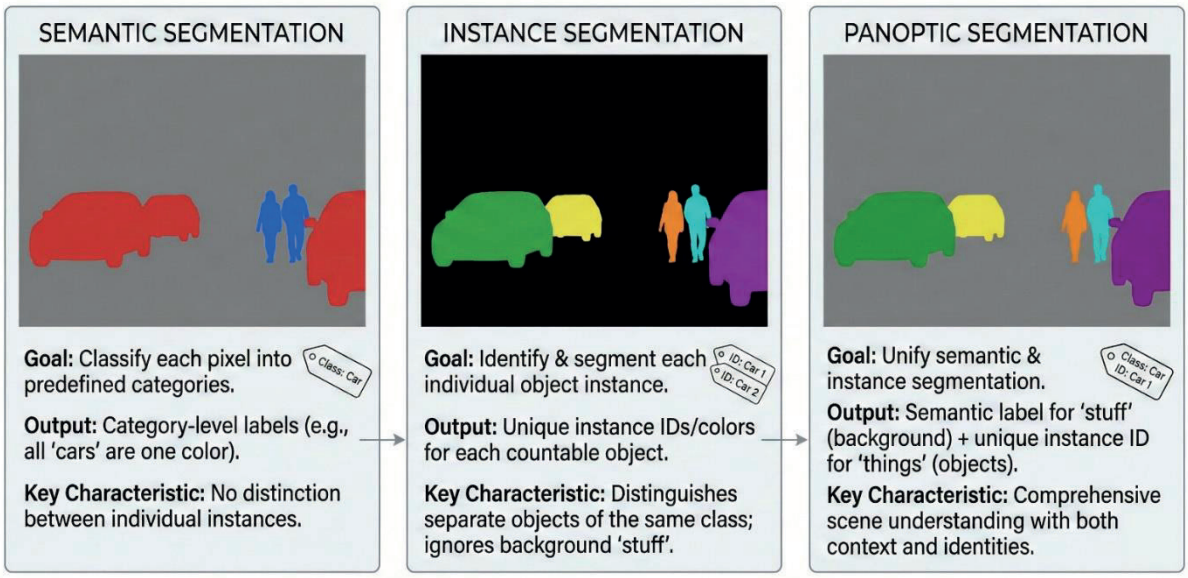

3. Context Capture in Deep Learning Architectures: DeepLab and the ASPP Module

In deep learning-based segmentation, standard convolutions often struggle to balance the trade-off between resolution and the receptive field, limiting the model's ability to capture long-range dependencies. To address this, the Atrous Spatial Pyramid Pooling (ASPP) module serves as a fundamental component of the DeepLab architecture. It is specifically designed to enhance semantic segmentation performance by overcoming these limitations. By utilizing multiple parallel atrous (or dilated) convolutions with varying rates, the ASPP module captures multi-scale contextual information effectively, which is crucial for understanding the spatial structures within complex images.

3.1 Technical Description of ASPP

The ASPP module consists of several parallel atrous convolution layers, each set to a different dilation rate. The dilation rate parameter dictates the spacing between kernel elements, effectively inserting zeros between filter weights. This mechanism expands the receptive field exponentially without reducing spatial resolution (down sampling) or increasing the number of parameters, thereby preserving dense feature maps essential for segmentation tasks. Standard implementations, such as DeepLabv3, typically employ parallel convolutions with rates of 1, 6, 12, and 18. A rate of 1 captures local, high-frequency details (standard convolution), while higher rates (e.g., 12, 18) capture long-range contextual dependencies, enabling the network to resolve scale variations across the image hierarchy (Wang et al., 2018; Zhang et al., 2019).

3.2 Multi-Scale Context Capture

In complex environments like urban streetscapes, objects exhibit extreme scale variations (e.g., distant traffic signs vs. nearby pedestrians). The ASPP module addresses this by probing the incoming feature map at multiple rates simultaneously. Low dilation rates preserve the boundaries of small structures, while high dilation rates integrate broad contextual cues necessary for recognizing large or occluded objects. By merging the outputs of these varied dilated convolutions, the ASPP combines fine-grained and broad contextual information into a comprehensive feature representation (Wang et al., 2018; Zhang et al., 2019). This allows the model to discern relationships between objects in the scene, improving the segmentation quality significantly.

3.3 Feature Fusion

The outputs of the different atrous convolutions within the ASPP module are then concatenated and processed through a 1x1 convolution layer to reduce dimensionality and enhance feature learning. This step is crucial as it consolidates diverse features extracted from various scales into a unified representation, allowing for more robust decision-making during the segmentation process.

Crucially, the module incorporates Image-Level Features via Global Average Pooling (GAP). This branch captures the global context of the entire image, resolving ambiguities that local receptive fields cannot address (e.g., distinguishing a road surface from a sidewalk based on the overall scene layout) (Zhao et al., 2024).

In conclusion, the ASPP module in the DeepLab architecture significantly enhances semantic segmentation by allowing for effective multi-scale feature extraction through parallel atrous

convolutions. By capturing contextual information at various scales and fusing these features, ASPP creates a comprehensive representation that is more informative for segmentation tasks. This capability enables models to perform better in complex scenarios featuring diverse object sizes and spatial arrangements. Figure 3 illustrates the architecture of ASSP.

Figure 3. The architecture of the ASPP module in DeepLab.

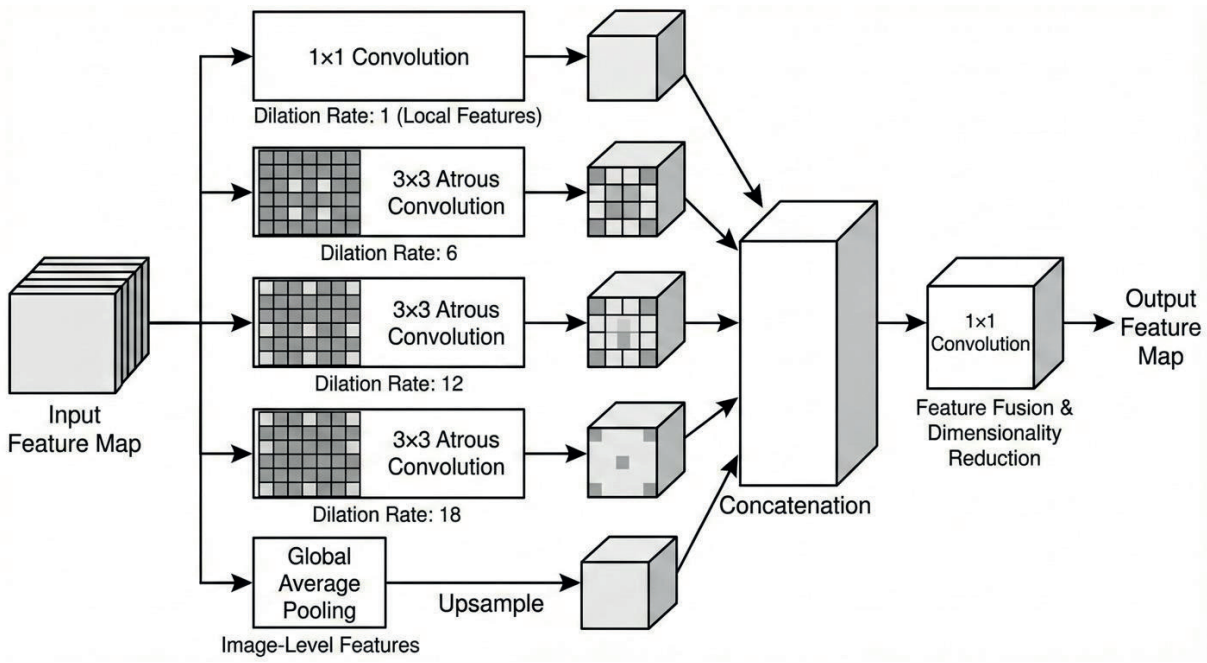

4. Addressing Class Imbalance: The Dice Loss Function

The Dice Loss function is a specialized loss function used in semantic segmentation, particularly effective in tasks where class imbalance is prevalent, such as segmenting small tumors from large medical scans. This function is grounded in the Dice coefficient, which is a statistical tool used to gauge the similarity between two sets. In the context of semantic segmentation, these sets represent the predicted segmentation mask and the ground truth mask.

4.1 Mathematical Formula

Mathematically, the Dice coefficient functions both as a validation metric for discrete sets and as a differentiable loss function ('Soft Dice') for training on probabilistic maps. The formulation is expressed as:

$$\text{Dice} = \frac{2\sum_i^N p_i g_i}{\sum_i^N p_i + \sum_i^N g_i + \epsilon}$$

Here, $p_i \in [0, 1]$ denotes the predicted probability that pixel i belongs to the target class, and $g_i \in \{0, 1\}$ represents the corresponding binary ground truth label. The smoothing factor ϵ is introduced to ensure numerical stability and prevent division by zero.

The Dice Loss function adapts this coefficient for optimization by minimizing the dissimilarity between prediction and ground truth:

$$\mathcal{L}_{\text{Dice}} = 1 - \frac{2\sum_i p_i g_i + \epsilon}{\sum_i p_i + \sum_i g_i + \epsilon}$$

This formulation transforms the maximization of overlaps into a minimization problem suitable for gradient descent optimization. Figure 4 visualizes the class imbalance.

Figure 4. Addressing Class Imbalance: Cross-Entropy vs. Dice Loss Mechanisms

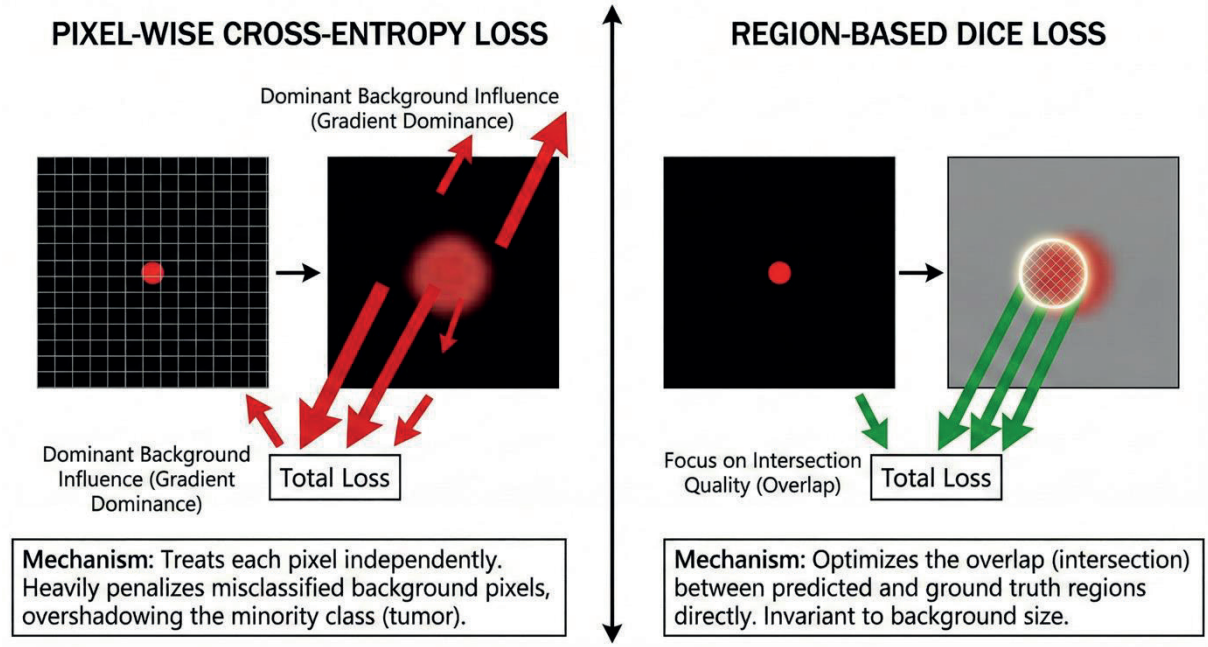

4.2 Advantages Over Pixel-Wise Cross-Entropy

Traditional pixel-wise cross-entropy loss functions treat each pixel independently and assign equal importance to every pixel. This can lead to significant issues in scenarios where the number of pixels in one class vastly outweighs the pixels in another class. In medical imaging, particularly when segmenting small tumors against a backdrop of healthy tissue, the discrepancy can be quite large:

1. In a typical medical scenario, especially those involving small tumors, the pixels corresponding to tumors may represent only a tiny fraction of the total pixels in an image. For instance, if a tumor occupies just a few pixels in a 512x512 pixel image, this equates to less than 1% of the entire image area. In scenarios with extreme class imbalance (e.g., a tumor occupying <1% of the image), standard Cross-Entropy Loss is susceptible to gradient dominance by the majority class. The accumulated gradients from the vast number of easy-to-classify background pixels overwhelm the sparse

signals from the tumor, causing the model to converge towards a local minimum where it predicts 'background' solely (Wen et al., 2023).

2. Unlike Cross-Entropy, which operates as a pixel-wise proxy, Dice Loss optimizes the intersection-over-union directly at the region level. This makes the loss value invariant to the size of the background, ensuring that the gradient signal is driven primarily by the overlap quality of the target object, regardless of how small it is relative to the image.
3. The formulation of Dice Loss inherently stresses the importance of accurate segmentation by rewarding true positives and balancing false positives and negatives. It facilitates improved training dynamics, particularly in the early stages of learning where the model is prone to making numerous errors, especially when classifying the minority class, which in this case comprises the tumor pixels (Wang et al., 2022).

5. Performance Evaluation: Mean Intersection over Union (mIoU)

To illustrate the calculation of the Mean Intersection over Union (mIoU), a simplified 3-class segmentation scenario is presented. This example utilizes a defined ground truth mask and a corresponding prediction mask to demonstrate the metric's computation. The process involves calculating the Intersection over Union (IoU) for each individual class, culminating in the derivation of the final mIoU score. Consider the following definitions:

For example, let's consider the following:

Classes:

Class 0: Background

Class 1: Class A

Class 2: Class B

Class 3: Class C

Consider a sample 3x3 image (9 pixels total) with 3 classes (0: Background, 1: Car, 2: Pedestrian).

Ground Truth (GT):

0 0 1
0 1 2
2 2 2

(Counts: Class 0=3, Class 1=2, Class 2=4. Total=9)

Prediction (Pred):

0 0 0
0 1 2
1 2 2

(Counts: Class 0=4, Class 1=2, Class 2=3. Total=9)

Step 1: Calculate IoU for Each Class

The IoU formula is defined as:

$$\text{IoU}(A, B) = \frac{|A \cap B|}{|A \cup B|} = \frac{\text{Intersection}}{\text{Union}}$$

where:

A is the count of pixels in the predicted segmentation corresponding to a specific class.

B is the count of pixels in the ground truth segmentation corresponding to that class.

Class 0 (Background)

Intersection: The count of pixels classified as background (0) in both the ground truth and the prediction maps. Based on the provided matrix, there is an overlap of 3 pixels between the prediction and the ground truth.

Ground Truth for Class 0: 3 pixels

Prediction for Class 0: 4 pixels

IoU Calculation:

$$\text{IoU}_0 = \frac{|A \cap B|}{|A \cup B|} = \frac{3}{3 + 4 - 3} = \frac{3}{4} = 0.75$$

Class 1 (Car) Analysis:

Intersection ($GT \cap Pred$): The pixel at position (1,1) matches. Count = 1.

Union ($GT \cup Pred$): GT(2) + Pred(2) - Int(1) = 3.

IoU: $1/3 \approx 0.33$

Class 2

Intersection: The number of overlapping pixels for Class 2. Based on our matrix, 3 pixels overlap.

Ground Truth for Class 2: 4 pixels

Prediction for Class 2: 3 pixels

IoU Calculation:

$$\text{IoU}_2 = \frac{3}{4 + 3 - 3} = \frac{3}{4} = 0.75$$

Step 2: Calculate the Mean Intersection over Union (mIoU)

The mIoU is defined as the average of the IoUs computed for each class.

$$\text{mIoU} = \frac{0.75 + 0.33 + 0.75}{3} = \frac{1.83}{3} = 0.61$$

where (N) is the number of classes (3 in this case).

mIoU Calculation:

Class 0 IoU: Intersection(3) / Union(4) = 0.75

Class 1 IoU: 0.33

Class 2 IoU: Intersection(3) / Union(4) = 0.75

$$mIoU = \frac{0.75 + 0.33 + 0.75}{3} = 0.61$$

Figure 5. Visual breakdown of the mIoU metric computation.

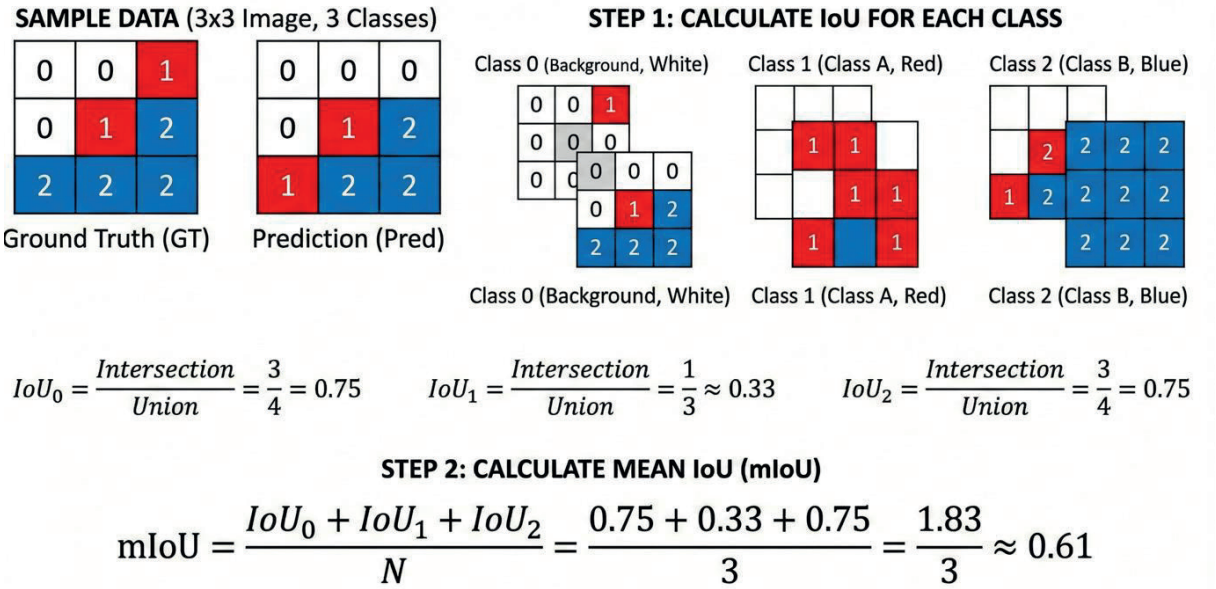

Figure 5 demonstrates the sample data, IoU calculation for each class and mean IoU calculation.

6. Semantic Segmentation in Autonomous Driving: Perception and Safety

Semantic segmentation plays a crucial role in enabling autonomous vehicles to understand and navigate their environments effectively. By providing a dense, pixel-level classification of the scene, it allows the vehicle's perception system to interpret complex visual data and make informed decisions.

6.1 Importance of Semantic Segmentation for Autonomous Vehicles

The segmentation process involves classifying every pixel in an image into distinct categories, which is vital for recognizing various elements critical to safe driving. Commonly segmented classes in the context of autonomous driving include:

1. Accurate segmentation of roadways, sidewalks, and parking areas is fundamental for defining the free space available for navigation. This ensures the vehicle adheres to safe traversable regions while avoiding restricted zones (Subhedar et al., 2023; Rahman et al., 2021).
2. Semantic segmentation delineates lane boundaries and road topology, which is critical for Lane Keeping Assist (LKA) systems and maintaining lateral control compliance with traffic regulations (Zhu et al., 2022; Taha & Hadi, 2024).
3. Semantic maps serve as critical input for trajectory prediction algorithms. For instance, classifying a pedestrian's orientation and location relative to a crosswalk enables the system to accurately anticipate future states and potential intersection points, providing the foundational data required for safety subsystems (Selee et al., 2023; Sun et al., 2020).
4. Recognizing other vehicles, whether stationary or in motion, is vital for collision avoidance and safe maneuvering. Segmentation helps differentiate these vehicles from other elements in the environment (Jebamikyous & Kashef, 2022; Wang et al., 2023).

6.2 Contribution to Path Planning and Safety Decisions

The dense understanding generated by semantic segmentation significantly contributes to path planning and safety mechanisms in autonomous vehicles:

- The data obtained through semantic segmentation feeds into the decision-making systems in real-time. The spatial data derived from semantic segmentation is directly integrated into the vehicle's control logic. For example, precise localization of pedestrians does not merely trigger detection but actively informs the velocity control module to initiate deceleration or emergency braking procedures (Kherraki et al., 2023; Muhammad et al., 2022). Furthermore, the delineation of static and dynamic obstacles allows the trajectory planner to compute optimal avoidance paths in real-time.
- Segmenting objects in the driving environment enables the vehicle to identify obstacles accurately and consider them when planning its trajectory. This is especially critical in dynamic environments where unexpected barriers may appear suddenly (Islam et al., 2019; Elamathiyan & Dhivya, 2024).
- By providing a map of the driving environment with semantic labels, the vehicle has enhanced situational awareness. This understanding allows the vehicle to execute complex maneuvers, such as changing lanes, making turns at intersections, or navigating through tight spaces (Herb et al., 2021; Jebamikyous, 2024).
- Semantic segmentation can also play a role in predicting the movement of different entities on the road (e.g., vehicles and pedestrians). For instance, recognizing a pedestrian moving toward a crosswalk allows the vehicle's system to react preemptively rather than reactively, improving overall safety (Selee et al., 2023; Peng et al., 2022).

Figure 6. The integration of semantic segmentation into the autonomous navigation pipeline.

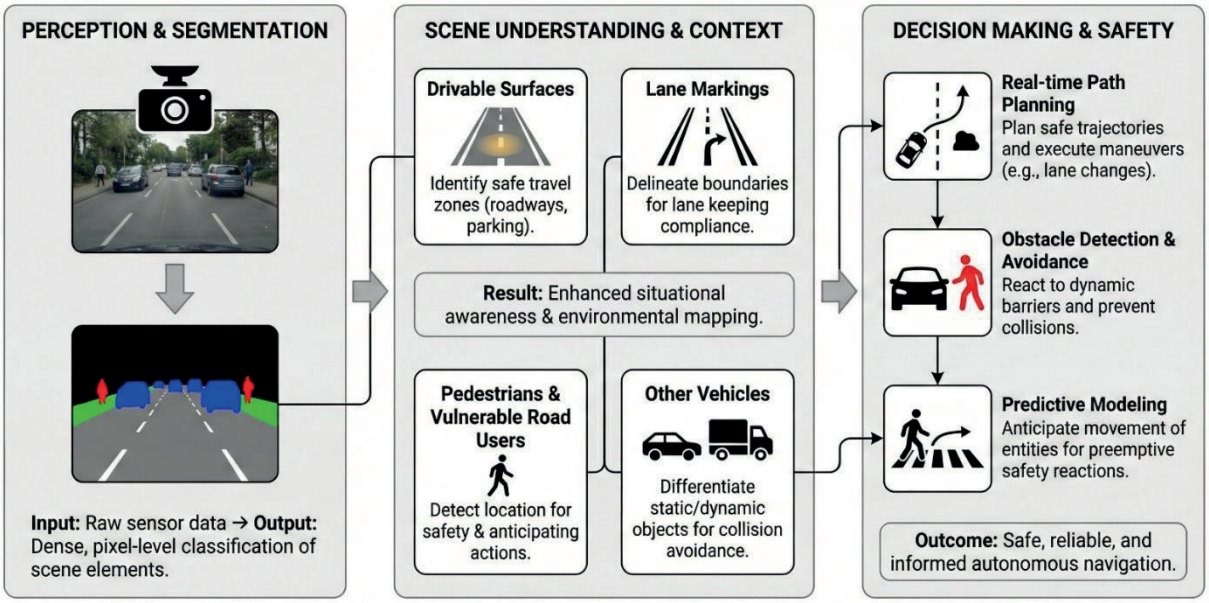

Figure 6 shows the integration of semantic segmentation for autonomous navigation.

7. Generalization Challenges: Domain Adaptation in Autonomous Driving

Domain adaptation (DA) is a critical concept in machine learning, particularly for tasks like semantic segmentation in autonomous driving. It focuses on transferring knowledge from a source domain, where labeled data is plentiful, to a target domain, where labeled data may be scarce or nonexistent. In the context of semantic segmentation for autonomous driving, this is essential as models trained on one dataset can struggle to generalize to other geographic locations due to differing environmental conditions, road types, and object appearances.

7.1 Challenges

A fundamental challenge in deployment is the 'domain gap'—the discrepancy between the training data distribution (Source Domain) and the operational environment (Target Domain). For example, a model trained on structured European roads (e.g., Cityscapes) may suffer significant performance degradation when deployed in unstructured environments due to covariate shifts in infrastructure and texture (Tsai et al., 2018).

Variations in weather across different regions can change the appearance of road surfaces and obstacles (e.g., snow, rain, or fog might obscure features that were easy to detect in the original training images). This can lead to discrepancies in how well the model interprets the environment (Chang et al., 2019).

The objects frequently encountered on streets (like vehicles, pedestrians, and cyclists) might have different appearances based on local contexts. The styles, colors, and shapes of vehicles, for instance, can vary significantly between regions (Zou et al., 2018).

Variations in lighting and time of day can also affect the feature distribution of images, complicating segmentation tasks. For example, images captured during bright daylight may be significantly different from those taken during twilight or at night (Zhang et al., 2024).

7.2 Strategies to Mitigate Domain Shift

To address these challenges, several strategies have been proposed for effective domain adaptation in semantic segmentation:

1. Unsupervised Domain Adaptation (UDA) techniques aim to leverage unlabeled data from the target domain and align it with features extracted from labeled source domain data. For instance, self-training methods can generate pseudo-labels on the target domain and use these for refining the segmentation model (Wang et al., 2020; Xie et al., 2021).
2. Feature-Level Alignment strategy aims to make the deep feature representations invariant to domain shifts. Adversarial training is commonly employed, where a domain discriminator forces the segmentation network to produce features that are indistinguishable between the source and target domains (Wang et al., 2021; Luo et al., 2019).
3. Category-Level Adaptation strategies focus on adapting the segmentation model at the category level. By understanding that certain classes dominate in one domain but not in another, models can be tailored to perform better on specific uncommon categories in the target domain (Yuan, 2022).
4. In contrast to feature-level alignment, Pixel-Level Alignment (Style Transfer) operates directly on the raw input data. Techniques such as Generative Adversarial Networks (GANs) transform source images to mimic the visual style (e.g., lighting, texture) of the target domain while preserving semantic content, effectively bridging the visual gap before the image enters the network (Wu et al., 2022; Luo et al., 2019).
5. Curriculum Learning is a structured approach where easier adaptation tasks are presented first. By gradually scaling the complexity, this method facilitates a smoother transition for models from the source to the target domain (Lian et al., 2019). This method allows the model to incrementally accommodate shifts in data distribution.

Figure 7. Strategies for bridging the domain gap in autonomous driving

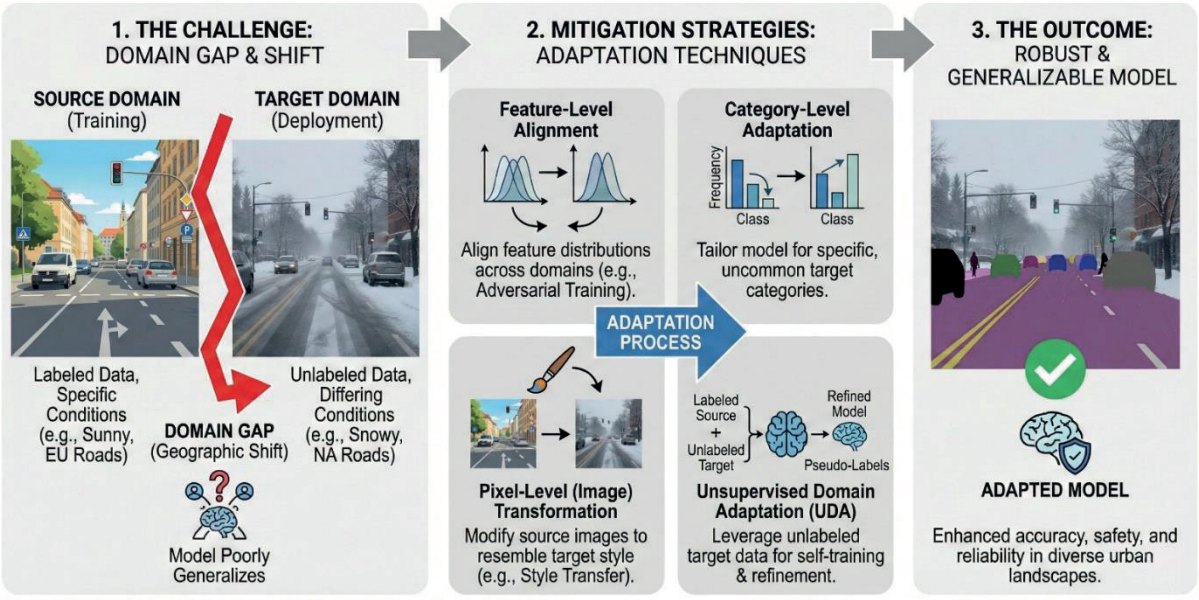

Domain adaptation is key for enhancing the performance of semantic segmentation models when deployed in new environments, addressing the discrepancies caused by geographical domain shifts. Figure 7 illustrates the strategies for bridging the domain gap.

8. Conclusions and Discussions

This chapter explores the multifaceted domain of semantic segmentation, establishing its role as a fundamental pillar in computer vision that transcends simple image processing to enable machine perception of complex environments. The evolution from classical methods to deep learning paradigms, particularly through Fully Convolutional Networks (FCNs), has marked a paradigm shift, allowing models to automatically learn hierarchical features and preserve spatial resolution more effectively than their predecessors.

A critical synthesis of segmentation methodologies reveals that while semantic segmentation provides essential categorical context, it is the development of instance and panoptic segmentation that has truly bridged the gap between recognizing "stuff" (amorphous regions) and "things" (countable objects). This distinction is paramount in dynamic applications like autonomous driving, where the system must not only classify a road surface but also distinguish between individual pedestrians and vehicles to ensure safe navigation and trajectory planning.

Architecturally, the integration of context has proven to be a decisive factor in model performance. The analysis of the DeepLab architecture and its Atrous Spatial Pyramid Pooling (ASPP) module demonstrates that capturing multi-scale contextual information is essential for resolving scale variations inherent in unconstrained environments. By utilizing parallel atrous convolutions, modern architecture can effectively fuse fine-grained details with broad contextual cues without compromising resolution. Furthermore, the discussion on loss functions highlights that standard pixel-wise cross-entropy is often insufficient in scenarios with extreme class imbalance, such as medical imaging. The adoption of Dice Loss addresses this by optimizing region-level overlap, ensuring that minority classes, such as small tumors, are not overwhelmed by background-dominant gradients.

Despite these advancements, the deployment of segmentation models in real-world scenarios faces significant challenges, primarily the domain gap. As highlighted, models trained on structured datasets often suffer performance degradation when exposed to the heterogeneity of novel environments characterized by differing weather, lighting, and infrastructure. The necessity for domain adaptation strategies, ranging from feature-level alignment to style transfer, underscores that achieving high mIoU scores on benchmark datasets is not sufficient for operational reliability. Future research must continue to focus on unsupervised domain adaptation and robust generalization techniques to ensure that semantic segmentation systems remain safe and effective across diverse and unpredictable urban landscapes.

Acknowledgements

The author acknowledges the use of artificial intelligence-assisted tools in the preparation of this chapter. Scite.ai was utilized to facilitate the literature search and ensure a comprehensive review of relevant studies. Gemini 3 Pro aided with grammatical refinement and stylistic enhancements to improve the clarity of the text. Additionally, NotebookLM was employed for the generation and conceptualization of the infographics presented herein. While these tools supported the drafting process, the author has thoroughly reviewed, verified, and edited all content and accepts full responsibility for the accuracy, originality, and integrity of the final manuscript.

References

Chang, W., Wang, H., Peng, W., & Chiu, W. (2019). All about structure: adapting structural information across domains for boosting semantic segmentation. https://doi.org/10.1109/cvpr.2019.00200

Cheng, B., Collins, M., Zhu, Y., Liu, T., Huang, T., Adam, H., … & Chen, L. (2019). Panoptic-deeplab. https://doi.org/10.48550/arxiv.1910.04751

Cheng, B., Misra, I., Schwing, A., Kirillov, A., & Girdhar, R. (2021). Masked-attention mask transformer for universal image segmentation. https://doi.org/10.48550/arxiv.2112.01527

Elamathiyan, A. and Dhivya, G. (2024). Explainable AI-based semantic object detection for autonomous vehicles., 15-32. https://doi.org/10.4018/979-8-3693-1962-8.ch002

Herb, M., Lemberger, M., Schmitt, M., Kurz, A., Weiherer, T., Navab, N., … & Tombari, F. (2021). Semantic image alignment for vehicle localization. https://doi.org/10.48550/arxiv.2110.04162

Islam, M., Chowdhury, M., Li, H., & Hu, H. (2019). Vision-based navigation of autonomous vehicles in roadway environments with unexpected hazards. Transportation Research Record Journal of the Transportation Research Board, 2673(12), 494-507. https://doi.org/10.1177/0361198119855606

Jebamikyous, H. (2024). Deep learning-based semantic segmentation in autonomous driving. https://doi.org/10.32920/25266736.v1

Jebamikyous, H. and Kashef, R. (2022). Autonomous vehicles perception (avp) using deep learning: modeling, assessment, and challenges. IEEE Access, 10, 10523-10535. https://doi.org/10.1109/access.2022.3144407

Kherraki, A., Maqbool, M., & Ouazzani, R. (2023). Efficient lightweight residual network for real-time road semantic segmentation. IAES International Journal of Artificial Intelligence (Ij-Ai), 12(1), 394. https://doi.org/10.11591/ijai.v12.i1.pp394-401

Kirillov, A., Girshick, R., He, K., & Dollár, P. (2019). Panoptic feature pyramid networks., 6392-6401. https://doi.org/10.1109/cvpr.2019.00656

Kong, V., Lee, E., Kim, K., & Shon, H. (2024). Integrating super-resolution with deep learning for enhanced periodontal bone loss segmentation in panoramic radiographs. Bioengineering, 11(11), 1130. https://doi.org/10.3390/bioengineering11111130

Li, J., Raventos, A., Bhargava, A., Tagawa, T., & Gaidon, A. (2018). Learning to fuse things and stuff. https://doi.org/10.48550/arxiv.1812.01192

Lian, Q., Duan, L., Lv, F., & Gong, B. (2019). Constructing self-motivated pyramid curriculums for cross-domain semantic segmentation: a non-adversarial approach., 6757-6766. https://doi.org/10.1109/iccv.2019.00686

Liu, A. and Yang, Y. (2023). A multilevel segmentation method of asymmetric semantics based on deep learning. IET Cyber-Physical Systems Theory & Applications, 9(2), 194-205. https://doi.org/10.1049/cps2.12075

Luo, Y., Liu, P., Guan, T., Yu, J., & Yang, Y. (2019). Significance-aware information bottleneck for domain adaptive semantic segmentation., 6777-6786. https://doi.org/10.1109/iccv.2019.00688

Luo, Y., Zheng, L., Guan, T., Yu, J., & Yang, Y. (2019). Taking a closer look at domain shift: category-level adversaries for semantics consistent domain adaptation., 2502-2511. https://doi.org/10.1109/cvpr.2019.00261

Muhammad, K., Hussain, T., Ullah, H., Ser, J., Rezaei, M., Kumar, N., … & Albuquerque, V. (2022). Vision-based semantic segmentation in scene understanding for autonomous driving: recent achievements, challenges, and outlooks. IEEE Transactions on Intelligent Transportation Systems, 23(12), 22694-22715. https://doi.org/10.1109/tits.2022.3207665

Peng, L., Chen, Z., Fu, Z., Liang, P., & Cheng, E. (2022). Bevsegformer: bird's eye view semantic segmentation from arbitrary camera rigs. https://doi.org/10.48550/arxiv.2203.04050

Rahman, Q., Sünderhauf, N., Corke, P., & Dayoub, F. (2021). Fsnet: a failure detection framework for semantic segmentation. https://doi.org/10.48550/arxiv.2108.08748

Selee, B., Faykus, M., & Smith, M. (2023). Semantic segmentation with high inference speed in off-road environments., 1. https://doi.org/10.4271/2023-01-0868

Subhedar, J., Bachute, M., Koundal, D., & Kotecha, K. (2023). Semantic segmentation algorithm for autonomous driving using unet architectures: a comparative study. https://doi.org/10.21203/rs.3.rs-2928293/v1

Sun, J., Zhang, Y., Zhu, J., Wu, J., & Kong, Y. (2021). Semi-supervised medical image semantic segmentation with multi-scale graph cut loss., 624-628. https://doi.org/10.1109/icip42928.2021.9506098

Sun, L., Yang, K., Hu, X., Hu, W., & Wang, K. (2020). Real-time fusion network for rgb-d semantic segmentation incorporating unexpected obstacle detection for road-driving images. https://doi.org/10.48550/arxiv.2002.10570

Taha, H. and Hadi, G. (2024). Semantic segmentation for self-driving cars., 99-103. https://doi.org/10.24086/cocos2024/paper.1537

Tsai, Y., Hung, W., Schulter, S., Sohn, K., Yang, M., & Chandraker, M. (2018). Learning to adapt structured output space for semantic segmentation. https://doi.org/10.1109/cvpr.2018.00780

Wang, Q., Dai, D., Hoyer, L., Fink, O., & Gool, L. (2021). Domain adaptive semantic segmentation with self-supervised depth estimation. https://doi.org/10.48550/arxiv.2104.13613

Wang, S., Jiang, Z., Yang, H., Li, X., & Yang, Z. (2022). Automatic segmentation of lumbar spine mri images based on improved attention u-net. Computational Intelligence and Neuroscience, 2022, 1-10. https://doi.org/10.1155/2022/4259471

Wang, W., He, H., & Ma, C. (2023). An improved deeplabv3+ model for semantic segmentation of urban environments targeting autonomous driving. International Journal of Computers Communications & Control, 18(6). https://doi.org/10.15837/ijccc.2023.6.5879

Wang, W., Xiong, Y., Yang, J., Su, M., Zhang, L., Yang, Z., … & Kuang, Y. (2022). Lidar-based real-time panoptic segmentation via spatiotemporal sequential data fusion. Remote Sensing, 14(8), 1775. https://doi.org/10.3390/rs14081775

Wang, Y., Liang, B., Ding, M., & Li, J. (2018). Dense semantic labeling with atrous spatial pyramid pooling and decoder for high-resolution remote sensing imagery. Remote Sensing, 11(1), 20. https://doi.org/10.3390/rs11010020

Wang, Z., Yu, M., Wei, Y., Feris, R., Xiong, J., Hwu, W., … & Shi, H. (2020). Differential treatment for stuff and things: a simple unsupervised domain adaptation method for semantic segmentation. https://doi.org/10.48550/arxiv.2003.08040

Wen, X., Liang, B., Zhao, B., Hu, X., Yuan, M., Hu, W., … & Xing, D. (2023). Application of fgd-bcel loss function in segmenting temporal lobes on localized ct images for radiotherapy. Frontiers in Oncology, 13. https://doi.org/10.3389/fonc.2023.1204044

Wu, J., Tang, Z., Xu, C., Liu, E., Gao, L., & Yan, W. (2022). Super-resolution domain adaptation networks for semantic segmentation via pixel and output level aligning. Frontiers in Earth Science, 10. https://doi.org/10.3389/feart.2022.974325

Xie, B., Yin, K., Li, S., & Chen, X. (2021). Spcl: a new framework for domain adaptive semantic segmentation via semantic prototype-based contrastive learning. https://doi.org/10.48550/arxiv.2111.12358

Yuan, B. (2022). Birds of a feather flock together: category-divergence guidance for domain adaptive segmentation. https://doi.org/10.48550/arxiv.2204.02111

Zhang, M., Zhao, J., Li, X., Li, Z., & Li, Q. (2019). Ascnet: adaptive-scale convolutional neural networks for multi-scale feature learning. https://doi.org/10.48550/arxiv.1907.03241

Zhang, X., Li, Y., Sheng, H., & Zhang, X. (2024). Adversarial unsupervised domain adaptation for 3d semantic segmentation with 2d image fusion of dense depth. Computer Graphics Forum, 43(7). https://doi.org/10.1111/cgf.15250

Zhao, S., Wang, Z., Huo, Z., & Zhang, F. (2024). Semantic segmentation network based on adaptive attention and deep fusion utilizing a multi-scale dilated convolutional pyramid. Sensors, 24(16), 5305. https://doi.org/10.3390/s24165305

Zhu, Y., Miao, C., Hajiaghajani, F., Huai, M., Su, L., & Qiao, C. (2022). Demo: attacking lidar semantic segmentation in autonomous driving. https://doi.org/10.14722/autosec.2022.23022

Zou, Y., Yu, Z., Kumar, B., & Wang, J. (2018). Unsupervised domain adaptation for semantic segmentation via class-balanced self-training., 297-313. https://doi.org/10.1007/978-3-030-01219-9_18

CHAPTER 2

ENERGY STORAGE AND FLEXIBILITY IN TURKEY'S POWER SYSTEM

Yelda KARATEPE MUMCU[1]

1 Assoc. Prof. Dr., Department of Electrical and Energy, Vocational School of Technical Sciences, Marmara University, Turkey. ORCID: https://orcid.org/0000-0001-9948-9413 email:ykaratepe@marmara.edu.tr

1. Introduction

As Turkey's energy system undergoes a significant transformation toward decarbonization and renewable expansion, the role of **grid flexibility** has become paramount. The share of renewables in total electricity generation reached approximately **42% by 2023**, with wind and solar energy accounting for more than 20% of total installed capacity [1]. However, this rapid uptake of variable renewable energy sources (vRES) has exposed the limitations of the current power system in managing intermittency and ensuring real-time balancing.

A central challenge is the **mismatch between supply and demand**, especially during peak solar generation or low wind availability. This mismatch amplifies the need for both **energy storage** and **flexibility services** such as frequency regulation, voltage support, and load shifting [2]. Without such capabilities, grid reliability is compromised, leading to potential curtailment of renewables and increasing reliance on fossil-based balancing reserves [3].

TEİAŞ, the national transmission system operator, has acknowledged this gap and incorporated storage into its **Electricity Transmission Master Plan (2021–2035)**, forecasting up to **7 GW of storage capacity need by 2035**, especially in regions with high solar and wind penetration [4]. Yet, deployment remains limited due to regulatory ambiguity, lack of bankable market mechanisms, and the absence of a dedicated storage framework [5].

Energy storage—particularly **grid-scale lithium-ion batteries and pumped hydro**—emerges as a critical solution to these flexibility constraints. Studies suggest that **even 2–3 GW** of strategically placed storage could significantly reduce balancing costs and enhance the integration of renewables in regions like the Aegean and Central Anatolia [6]. Furthermore, **distributed storage systems** (e.g., behind-the-meter batteries in industrial zones) offer additional benefits for local grid congestion relief and prosumer empowerment [7].

Globally, countries such as Germany, the UK, and Australia have advanced storage-supportive regulatory models, including capacity remuneration, fast frequency response (FFR) markets, and co-location incentives. Turkey's policy development must consider these international benchmarks to avoid lock-in effects and facilitate a smooth flexibility transition [8].

This chapter explores the evolving landscape of energy storage and flexibility in Turkey, examining technical potentials, market barriers, policy dynamics, and pilot projects. By identifying institutional and infrastructural bottlenecks, it aims to present an actionable roadmap to embed energy storage within the heart of Turkey's electricity reform (Figure 1).

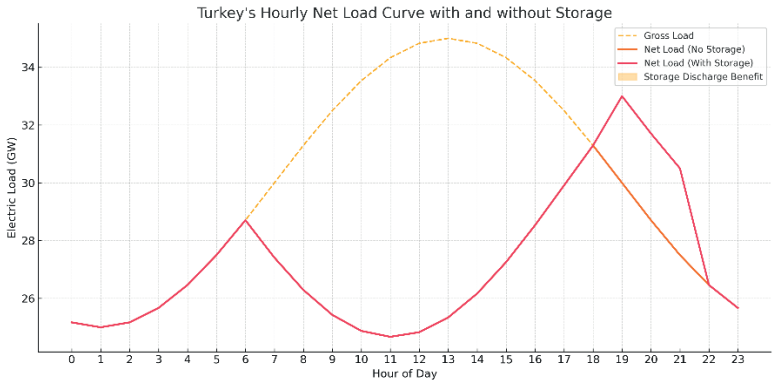

Figure 1. Turkey's Hourly Net Load Curve with and without Storage.

2. Current Challenges with Renewable Integration

Turkey's rapid expansion of renewable energy—especially solar and wind—has introduced significant operational, infrastructural, and regulatory challenges for its electricity system. By 2023, Turkey's total installed renewable capacity surpassed 58 GW, representing over 54% of total capacity, yet much of this remains underutilized due to grid congestion and curtailment risks [9].

Renewables in Turkey are geographically concentrated in high-resource regions like the Aegean, Southeastern Anatolia, and Central Anatolia. However, transmission infrastructure in these regions often lags behind generation growth. According to TEİAŞ's latest reports, over 2.3 GW of wind and solar projects faced delays or output limitations due to congestion in 2022 [10]. This has led to a rise in renewable energy curtailment, reducing economic efficiency and investor confidence [11].

The increasing share of variable renewable energy (VRE) has made day-ahead and intraday forecasting accuracy a system-critical issue. TEİAŞ's balancing market performance metrics show that forecast errors exceed 8–10% for wind and solar during high-variability periods [12]. This shortfall increases balancing costs and reliance on fossil-based peaking plants.

Turkey lacks a dedicated market for fast-response ancillary services. Currently, primary and secondary frequency reserves are mainly provided by natural gas units. This setup is not only carbon-intensive but also inflexible under high VRE scenarios [13].

Although the 2021–2035 Transmission Master Plan outlines ambitious goals for renewable integration, project execution is often hindered by permitting bottlenecks, connection queue delays, and inflexible grid codes [10], [14]. There's a pressing need to align regulatory timelines with actual project development cycles.

These systemic issues underline the urgent requirement for flexibility-enhancing mechanisms, including energy storage, demand response, and advanced grid forecasting. As shown in Figure 2, without adequate storage or flexible resources, net load volatility places increasing stress on the national grid, especially during evening peak hours (Figure 2).

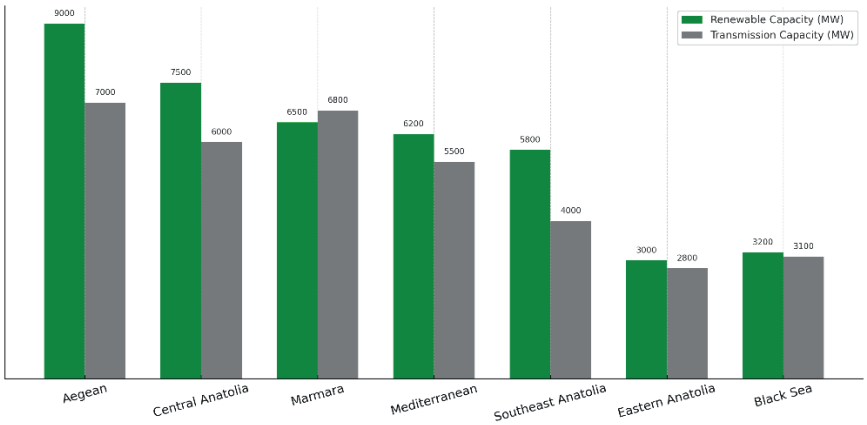

Figure 2. Regional Mismatch Between Renewable and Transmission Capacity in Turkey.

3. Energy Storage Technologies: Current Status and Potential in Turkey

The integration of renewable energy at scale requires not only new generation capacity but also flexible technologies capable of addressing variability and balancing challenges. Among these, energy storage systems (ESS) have emerged as a cornerstone of future-proof power systems. Turkey, despite being a late mover in this field, is now showing increasing momentum in both policy and pilot deployment of storage technologies.

3. 1. Battery Energy Storage Systems (BESS)

Lithium-ion battery systems are globally dominant due to their scalability, rapid response, and falling costs. In Turkey, battery storage has gained traction following regulatory changes introduced by EMRA in 2022, which allowed storage to be co-located with generation under the "pre-license" model [15]. By mid-2023, more than 12 GW of battery storage license applications had been submitted, indicating immense interest from the private sector [16]. However, the majority of these are speculative and await market clarity regarding remuneration mechanisms.

Utility-scale BESS projects remain limited. A few pilot projects—such as TEİAŞ's integration studies with hybrid solar + storage units in Konya and Sanliurfa—are currently under technical review. The long-term potential is estimated at 5–7 GW of battery storage by 2035, especially in solar-dominant regions [17].

3.2 Pumped Hydro Storage

Turkey has a large hydroelectric base (~30 GW), but pumped hydro storage (PHS) is underdeveloped. Unlike many EU countries, no utility-scale PHS facility exists, though multiple feasibility studies have been conducted on reservoirs like Oymapinar and Deriner [18]. The main barrier has been high capital cost, long lead times, and lack of capacity market signals.

Nevertheless, the National Energy Plan (2023) includes PHS within its 2053 climate neutrality strategy. If supported through public-private partnerships and green finance instruments, up to 2 GW of pumped storage could be operational by 2040 [19].

3.3. Distributed and Behind-the-Meter Storage

Industrial zones, Organized Industrial Zones (OIZ), and commercial consumers are exploring behind-the-meter battery systems to optimize self-consumption and reduce peak tariffs. Coupled with rooftop solar PV, this segment is expected to grow rapidly with the development of net billing mechanisms and time-of-use pricing schemes (Table 1) [20].

Table 1. Technology Comparison and Suitability

STORAGE TYPE	ADVANTAGES	KEY BARRIERS
LITHIUM-ION BATTERY	Fast response, modular, declining cost	Grid code adaptation, financing
PUMPED HYDRO	High capacity, long duration	High capex, long permitting
DISTRIBUTED STORAGE	Consumer empowerment, peak shaving	Lack of incentives, market access

Overall, energy storage in Turkey is at a policy and market inflection point**.** The speed at which clear remuneration models, grid services markets, and investment frameworks are established will determine whether Turkey can meet its renewable integration and flexibility goals by 2035.

Figure 3 illustrates the current installed capacity and pipeline projects for battery storage, pumped hydro, and distributed BESS. While installed capacity remains limited, policy momentum has driven significant licensing applications, particularly for grid-scale batteries.

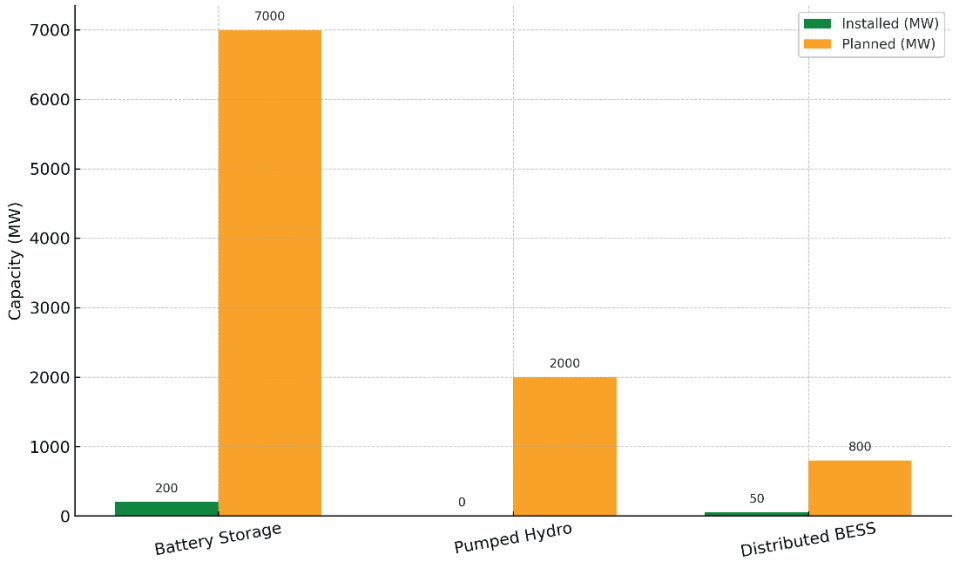

Figure 3. Installed and Planned Energy Storage Projects in Turkey by Type

4. Policy and Regulatory Framework for Energy Storage and Flexibility

4.1. Institutional and Governance Structure

Turkey's regulatory framework for energy storage is shaped primarily by two core institutions:

- **Energy Market Regulatory Authority (EMRA)** – Develops licensing procedures, sets tariffs, and enforces electricity market rules, including recent regulations enabling co-located storage systems.
- **Turkish Electricity Transmission Corporation (TEİAŞ)** – Oversees grid operations, system planning, and ancillary service provision.

Both institutions are responsible for aligning national energy policy with flexibility and decarbonization objectives.

4.2. Recent Legislative Developments

A major milestone occurred in November 2022, when EMRA issued a long-anticipated amendment to the Electricity Market Law. The reform allows:

- Storage-integrated renewable generation to obtain single pre-licenses
- Storage systems to charge from the grid and participate in electricity markets
- Prospective engagement in balancing and reserve services

These legal changes aim to accelerate storage deployment and unlock investor interest [21].

4.3. Current Market Design Challenges

Despite regulatory progress, several barriers persist in market structure:

- No capacity remuneration mechanism for storage
- Lack of dedicated ancillary service markets (e.g., frequency regulation)
- Absence of net billing or time-of-use tariffs for distributed storage
- No standardized valuation of flexibility services

These gaps create uncertainty for both utility-scale and distributed storage investors [22], [23].

4.4. Alignment with Global Best Practices

In leading jurisdictions like the UK, Germany, and Australia, energy storage is recognized as a standalone grid asset eligible for multiple revenue streams. These include:

- Capacity markets
- Fast Frequency Response (FFR) auctions
- Reactive power and black start services

Global agencies such as IRENA and the World Bank recommend Turkey develop similar frameworks to attract investment and avoid market distortion [24].

4.5. Ongoing and Planned Regulatory Actions

TEİAŞ and EMRA are preparing further reforms to improve grid flexibility, including:

- Flexibility Roadmap (2024–2026) – to define storage services, procurement mechanisms, and pilot incentives
- Reform of the balancing and reserve markets to allow battery participation
- New regulatory sandboxes and pilot zones for storage technologies [25]

These initiatives are expected to be implemented in phases starting in 2024.

5. Roadmap and Policy Recommendations for Flexibility Transition

To ensure a secure and renewable-driven electricity system, Turkey must adopt a structured and forward-looking flexibility roadmap that prioritizes regulatory reform, market innovation, and system-level coordination. This section outlines an integrated strategy spanning short-, mid-, and long-term horizons.

In the short term (2024–2026)**,** the priority should be finalizing EMRA's regulatory framework on storage and flexibility services, including updating relevant grid codes to enable full participation of storage units in balancing and ancillary services. TEİAŞ should initiate pilot markets for fast frequency response and ramping reserves, particularly targeting battery storage. Additionally, regulatory sandboxes should be introduced to support innovation in distributed storage applications for industrial and commercial consumers. To accelerate deployment,

government-backed or blended financing mechanisms should be established to fund initial storage demonstration projects.

Looking toward the mid-term period (2027–2030), Turkey will need to establish a capacity remuneration mechanism that provides long-term investment signals for flexible assets such as batteries, pumped hydro, and demand response. Time-of-use tariffs and net billing mechanisms should be adopted to incentivize consumer-level storage investments, particularly in commercial and organized industrial zones. The regulatory framework must also evolve to recognize multi-service business models for storage, allowing operators to stack value streams such as arbitrage, black-start capability, and ancillary services. Furthermore, TEİAŞ's integrated resource planning processes should be updated to incorporate storage solutions into regional congestion and investment analyses.

In the long term (2030–2035), Turkey should target a minimum of 10 GW of cumulative storage capacity, including both utility-scale and distributed systems. This will require scaling up smart grid infrastructure, grid digitalization, and data-driven system operations. Additionally, the Turkish flexibility framework should be harmonized with European Union directives—such as RED III and the Electricity Regulation (EU) 2019/943—to support cross-border compatibility and facilitate access to green finance.

Effective governance is critical for executing this roadmap. A national Flexibility Task Force should be established under the Ministry of Energy and Natural Resources (MENR), bringing together EMRA, TEİAŞ, TÜBİTAK, and private sector stakeholders. This body would be responsible for monitoring progress, coordinating between institutions, and resolving regulatory overlaps. Planning processes must be aligned with long-term investment cycles, and TEİAŞ should adopt performance-based metrics to prioritize grid resilience and system flexibility. Increasing transparency in project queues and market access—especially for hybrid and storage projects—is essential to unlock investor confidence.

Through this strategic and phased approach, Turkey can build a resilient, flexible, and renewable-ready power system by 2035, while aligning with global decarbonization and energy transition trends. In Figure 4, this roadmap outlines a phased strategy to support the integration of energy storage and system flexibility in Turkey's electricity market. It highlights short-term regulatory actions, mid-term market design reforms, and long-term deployment goals including smart grid scaling and EU alignment. The roadmap reflects the evolving priorities of EMRA and TEİAŞ, and serves as a reference for national policy implementation timelines.

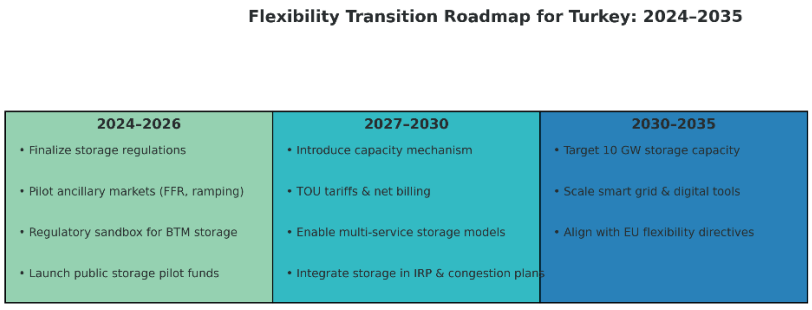

Figure 4. *Flexibility Transition Roadmap for Turkey (2024–2035).*

6. Conclusion

As Turkey moves toward a cleaner and more resilient power system, energy storage and grid flexibility emerge not merely as supportive technologies, but as foundational elements for future electricity infrastructure. The country's increasing share of renewable energy, particularly from variable sources such as solar and wind, necessitates a paradigm shift in how the grid is planned, operated, and regulated.

While recent regulatory reforms—such as the licensing of storage-integrated generation—mark important progress, Turkey must accelerate efforts to establish comprehensive market mechanisms, institutional coordination, and digital system capabilities. The transition to a flexible grid is not only a technical or economic necessity but also a strategic imperative for ensuring long-term energy security and climate alignment.

By implementing a structured roadmap, investing in enabling technologies, and aligning with international best practices, Turkey has the opportunity to become a regional leader in storage-based flexibility solutions. However, the success of this transition will depend on consistent policy signals, active stakeholder engagement, and long-term planning commitment.

References

Şahin, U., & Gürkan, S. (2023). Renewable Energy Integration and Grid Planning in Turkey. Energy Policy, 175, 113456.

Öztürk, M. & Tüfekci, P. (2021). The Value of Flexibility in Turkish Power Markets. Renewable and Sustainable Energy Reviews, 144, 110985.

IEA. (2022). Turkey 2022: Energy Policy Review. International Energy Agency.

TEİAŞ. (2021). 2021–2035 Electricity Transmission Master Plan. Ankara: TEİAŞ.

Aydemir, E., & Özdemir, M. (2020). Energy Storage Regulation and Investment Barriers in Turkey. Utilities Policy, 66, 101117.

Gürbüz, A., & Demirbaş, A. (2022). Scenario-based Modelling of Storage Integration for Turkey. Applied Energy, 310, 118493.

Korkmaz, H., & Sefer, A. (2023). Distributed Energy Storage and Demand Response in Turkish Grids. Energy Reports, 9, 2157–2169.

World Bank. (2023). Energy Storage Deployment and Policy Lessons. Washington, DC.

IEA. (2023). Renewable Energy Market Update: Turkey Focus. International Energy Agency.

TEİAŞ. (2022). Annual Grid Operation Report. Ankara.

Demir, Y., & Kara, M. (2021). Curtailment Risk in Turkey's Wind Sector. Energy Policy, 157, 112546.

Bilgin, A., & Yıldız, H. (2022). Forecast Accuracy and System Costs in Turkish Electricity Market. Renewable Energy, 188, 367–376.

Özcan, B., & Gözen, M. (2023). Ancillary Services Market Reform for Turkey's Power Sector. Utilities Policy, 83, 101520.

EMRA. (2022). Electricity Market Monitoring Report. Ankara: EMRA.

EMRA. (2022). *Regulatory Framework for Storage-Integrated Generation*. Ankara: EMRA.

Gözen, M., & Demirtaş, A. (2023). Battery Storage Licensing Trends in Turkey. *Energy Reports*, 9, 2432–2444.

TEİAŞ. (2023). *Storage Potential Assessment Study for Turkey*. Ankara.

Özkan, B. (2021). Feasibility of Pumped Hydro Energy Storage in Turkish Reservoirs. *Renewable Energy*, 169, 345–357.

Ministry of Energy and Natural Resources. (2023). *National Energy Plan 2023–2053*.

Sarı, E., & Yılmaz, T. (2022). Behind-the-Meter Storage and Industrial Demand in Turkey. *Journal of Cleaner Production*, 376, 134218.

EMRA. (2022). *Regulation on Electricity Storage Integrated Generation*. Official Gazette, 31900.

Gözen, M., & Karakaya, E. (2023). Regulatory Barriers to Grid-Scale Storage in Turkey. *Energy Strategy Reviews*, 48, 101082.

Aydın, B., & Yıldırım, M. (2022). Market Design Challenges for Flexibility Assets in Turkey. *Utilities Policy*, 79, 101416.

World Bank & IRENA. (2023). *Storage Market Design in Emerging Power Systems*.

TEİAŞ. (2023). *2024–2026 Flexibility Market Development Roadmap – Draft for Consultation*.

EMRA. (2023). *Draft Regulation on Flexibility Services and Storage Participation*.

World Bank. (2023). *Policy Pathways for Flexible Grids in Emerging Economies*.

IRENA. (2022). *Electricity Storage Valuation Frameworks*.

TEİAŞ. (2023). *Strategic Investment Planning Report 2024–2030*.

European Commission. (2023). *REPowerEU & RED III Guidelines for Member States*.

CHAPTER 3

EFFECT OF COIL–WORKPIECE DISTANCE AND COIL HEIGHT ON INDUCTION HEATING CHARACTERISTICS

İlyas ÖZER[1], Harun ÖZBAY[2], Adem DALCALI[3]

1 Doç. Dr., Bandırma Onyedi Eylül University, Department of Computer Engineering, Bandırma. iözer@bandirma.edu.tr
2 Doç. Dr., Bandırma Onyedi Eylül University, Department of Electrical Engineering, Bandırma. hozbay@bandirma.edu.tr
3 Doç. Dr., Bandırma Onyedi Eylül University, Department of Electrical and Electronics Engineering, Bandırma. adalcali@bandirma.edu.tr

1. Introduction

Induction heating is a heating technique that enables the contactless heating of materials through electromagnetic fields. In this method, heat is generated not by conduction from an external source, but as a result of eddy currents induced within the workpiece and magnetic hysteresis losses (Rudnev et al., 2017; Davies, 1990; Lupi et al., 2014). The generation of heat directly inside the material provides induction heating with distinct advantages such as high energy efficiency, short processing time, uniform heat distribution, and precise controllability. Compared to conventional heating systems, the elimination of safety risks such as combustion and explosion, along with the absence of waste generation after processing, makes induction heating a sustainable and preferred solution for both industrial and domestic applications, including surface hardening, metal melting, annealing, and household use (Lucia et al., 2014; Dalcalı et al., 2020).

In induction heating systems, a time-varying magnetic field is generated around the coil carrying an alternating current, in accordance with Faraday's law. This varying magnetic field induces closed-loop currents in the target region, referred to as the workpiece. As a result of these induced eddy currents, resistive (Joule) losses occur due to the electrical resistance of the material, which are directly converted into thermal energy. In addition to these losses, magnetic hysteresis losses also contribute to the overall heat generation within the material.

In induction heating systems, the influence of coil geometry on the electromagnetic field distribution and the resulting heat generation has been extensively investigated in the literature using the finite element method (Wang et al., 1992). These studies demonstrate that induction heating performance depends not only on the supply parameters but also on the geometric characteristics of both the coil and the workpiece. Among the studies addressing the effects of coil geometry, Tavakoli et al. employed the finite element method to reveal the decisive role of coil cross-sectional shape, coil radius, and inter-turn spacing on magnetic field intensity and volumetric heat generation (Tavakoli et al., 2009). Similarly, Patil et al. reported through numerical analyses conducted for different helical coil geometries (conventional, conical, square, and oval) that coil shape directly influences magnetic flux distribution, thereby determining temperature uniformity within the workpiece (Patil et al., 2023). These findings highlight coil design as a critical factor in controlling end effects and localized overheating in induction heating systems.

The application-specific effects of coil geometry have also been examined in detail for processes such as brazing and welding. Zhao et al. analyzed different coil configurations in the induction brazing of copper–steel pipes using three-dimensional coupled electromagnetic–thermal models and demonstrated that coil structure plays a decisive role in heating efficiency and temperature uniformity (Zhao et al., 2021). Similarly, FEM-based studies developed for induction brazing applications have shown that the number of coil turns and the magnetic coupling between the coil and the workpiece directly affect heating performance (Khazaal et al., 2016).

Studies focusing on process parameters have primarily emphasized optimization approaches aimed at improving the energy efficiency of induction heating systems. Park and Dang demonstrated that significant energy savings can be achieved in an in-line induction heating process by optimizing parameters such as voltage and frequency using design of experiments and genetic algorithm–based methods (Park et al., 2012). Such studies reveal that induction heating systems represent a multivariable optimization problem, governed not only by geometric factors but also by operating parameters.

In studies addressing the physical fundamentals of induction heating, coupled modeling of electromagnetic and thermal fields has been a major focus. Sadeghipour et al. developed finite element models that account for temperature-dependent magnetic and thermal material properties and demonstrated that heating behavior changes significantly, particularly in the vicinity of the Curie temperature (Sadeghipour et al., 1996). Similarly, electromagnetic–thermal coupled models developed for surface hardening applications have quantitatively revealed the effects of induction parameters on hardening depth and temperature distribution (Sönmez, 2022).

The influence of workpiece geometry has also been an important topic of investigation in the literature. Tavakoli et al. reported that the ratio between workpiece height and coil length plays a decisive role in magnetic field distribution and ohmic loss profiles, and that inappropriate ratios lead to excessive heating in the end regions (Tavakoli et al., 2011). Similarly, studies examining the induction heating of work rolls in rolling applications have demonstrated that parameters such as coil–roll gap and operating frequency are critical for achieving surface temperature uniformity (Bao et al., 2018).

In recent years, innovative coil designs and magnetic field guidance approaches aimed at enhancing induction heating efficiency have increasingly appeared in the literature. Cui et al. proposed a focused induction heating method that concentrates the internal magnetic field of the coil by reducing magnetic flux leakage, and demonstrated that this approach provides a significant efficiency improvement compared to conventional systems (Cui et al., 2022). In addition, studies focusing on coils fabricated with litz wire have shown that more controlled and efficient heating at high temperatures can be achieved by mitigating skin and proximity effects (Patidar et al., 2018).

Overall, studies in the literature indicate that the performance of induction heating systems is strongly dependent on the interaction between coil geometry, workpiece dimensions, and process parameters (Wang et al., 1992; Patil et al., 2014). In this context, a systematic investigation of the effects of axial geometric parameters, such as coil length, on magnetic field distribution, current density, and ohmic loss profiles addresses an important gap in the literature and contributes to the design of more homogeneous and efficient induction heating systems.

A review of the studies conducted on induction heating systems in the literature reveals that the influence of coil geometry on electromagnetic field distribution, and consequently on thermal energy generation, has primarily been analyzed in terms of parameters such as coil cross-sectional shape, turn spacing, coil radius, and coil–workpiece distance. Although these studies demonstrate a strong correlation between induction heating efficiency and geometric design, it has been observed that investigations treating the axial dimension (length) of the coil as a systematic and independent design variable remain limited. Particularly in the induction heating of cylindrical and elongated workpieces, the coil length is known to directly affect the distribution of the magnetic field, the induced eddy current patterns, and consequently the homogeneity of ohmic loss density.

This study systematically investigates the effects of coil length and coil–workpiece distance on magnetic flux density, current density, and ohmic loss distributions in induction heating systems. To this end, the coil length and the coil–workpiece gap were varied over specified ranges, and the resulting redistribution of the electromagnetic field and heat source along the workpiece was examined in detail. The findings are expected to provide valuable design input for the homogeneous, controlled, and energy-efficient design of induction heating systems.

2. Induction Heating Systems

In induction heating systems, as illustrated in Figure 1, the time-varying magnetic field generated by a coil supplied with alternating current induces eddy currents in the workpiece when it intersects the material, in accordance with Faraday's law. These eddy currents produce ohmic losses due to the electrical resistance of the material, thereby converting electrical energy into thermal energy. In addition, in ferromagnetic materials, hysteresis losses arising from the reorientation of magnetic domains also contribute to the total heat generation. The total loss generated within the workpiece, and thus the resulting heating performance, can be considered as a function of the applied current amplitude, operating frequency, coil geometry, and the electromagnetic properties of the workpiece (Dalcalı et al., 2020).

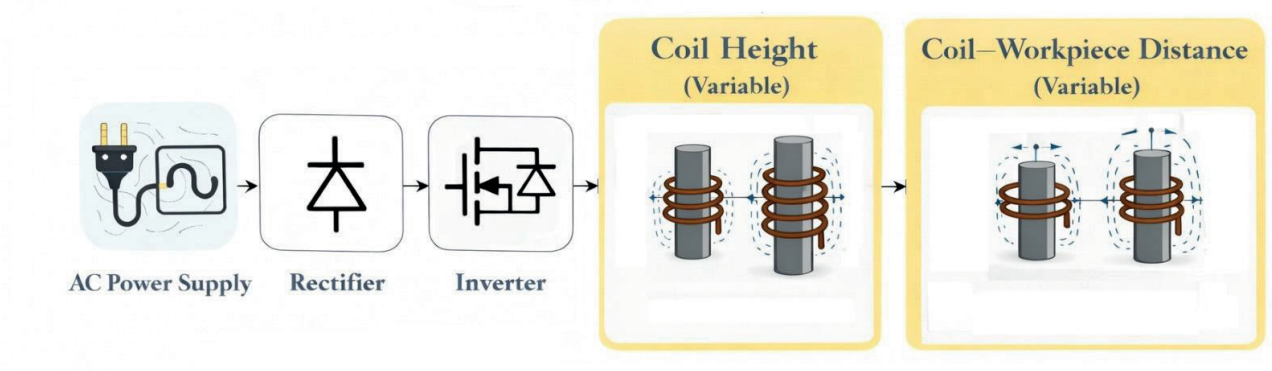

Figure 1. Schematic representation of the induction heating system.

2.1.Theoretical background

In an induction heating system, the voltage applied to the coil is expressed by Equation 1.

$$v(t) = V_0 \sin(\omega t) \tag{1}$$

This voltage generates a time-varying magnetic field around the coil. The resulting variable magnetic field induces eddy currents in the workpiece in accordance with Faraday's law, as expressed by the corresponding Equation 2 (Rudnev et al., 2017; Davies, 1990; Dalcalı et al., 2020).

$$v \oint_r E.d_\iota = -\frac{d\Phi}{dt} \tag{2}$$

In the equation, E denotes the induced electric field and, Φ represents the magnetic flux. In a conductive medium, where σ denotes the electrical conductivity, the current density is expressed as: (Rudnev et al., 2017; Lupi et al., 2014).

$$J = \sigma E \tag{3}$$

as defined by this expression. The ohmic (Joule) losses arising from the electrical resistance of the material and released in the form of heat are a direct consequence of these currents. The total power loss in the workpiece is expressed by Equation 4 (Lupi et al., 2014; Zinn and Semiatin, 1988).

$$P_j = \int_v \frac{J^2}{\sigma} dV \tag{4}$$

In ferromagnetic materials, in addition to eddy current–related losses, hysteresis losses are generated and are defined per unit volume by Equation 5 (Bertotti, 1998; Cullity and Graham, 2011).

$$W_h = \oint H \, dB \tag{5}$$

Therefore, in induction heating systems, the total loss generated within the workpiece is expressed by Equation 6 (Rudnev et al., 2017; Lupi et al., 2014; Bertotti, 1998; Cullity and Graham, 2011).

$$P_{total} = \frac{J^2}{\sigma} + f \oint H \, dB \tag{6}$$

As can be seen from Equation 6, the current applied to the coil, the operating frequency, the coil geometry, and the properties of the workpiece affect the heating performance.

Another phenomenon influenced by frequency is the skin effect. In a workpiece subjected to an alternating magnetic field, an increase in frequency leads to a reduction in the penetration depth defined by Equation 7, causing heat generation to be concentrated in regions close to the surface (Dalcalı et al., 2020).

$$\delta = \sqrt{\frac{2}{\omega \mu \sigma}} \tag{7}$$

2.2.The designed system

In this section, the induction heating system designed in accordance with the electromagnetic induction principles presented in the previous section is introduced. During the design process, particular emphasis was placed on the effects of coil geometry and the coil–workpiece distance on electromagnetic field distribution and the resulting heat generation. The system was modeled using the finite element method in order to clearly capture the physical behavior of the induction heating mechanism.

The designed induction heating system consists of an induction coil supplied with alternating current, a cylindrical workpiece, and an air region defined for the solution of the electromagnetic field. Owing to the axial symmetry of the system, it was modeled using a two-

dimensional axisymmetric approach, which preserves physical accuracy while reducing computational cost. The eddy current solution type was employed for the electromagnetic field analysis, as this approach enables accurate calculation of induced eddy currents and the associated ohmic losses in induction heating systems (Du et al., 2020). The geometric model consists of a workpiece with fixed dimensions and an induction coil whose parameters are varied. In this study, the geometry of the workpiece was kept constant, while the parameters defined in Table 1 were varied in order to investigate their effects on system performance.

Table 1. Minimum and Maximum Limits of the Parameters

Parameter	Lower bound (mm)	Upper bound (mm)	Step size (mm)
Coil length (H)	25	125	25
Distance between coil and workpiece (x)	1	7	1

In the FEM model shown in Figure 2, copper was used for the coil, while stainless steel was selected for the workpiece. An excitation of 1000 At at a frequency of 10 kHz was applied to the coil. The workpiece was designed with a length of 100 mm.

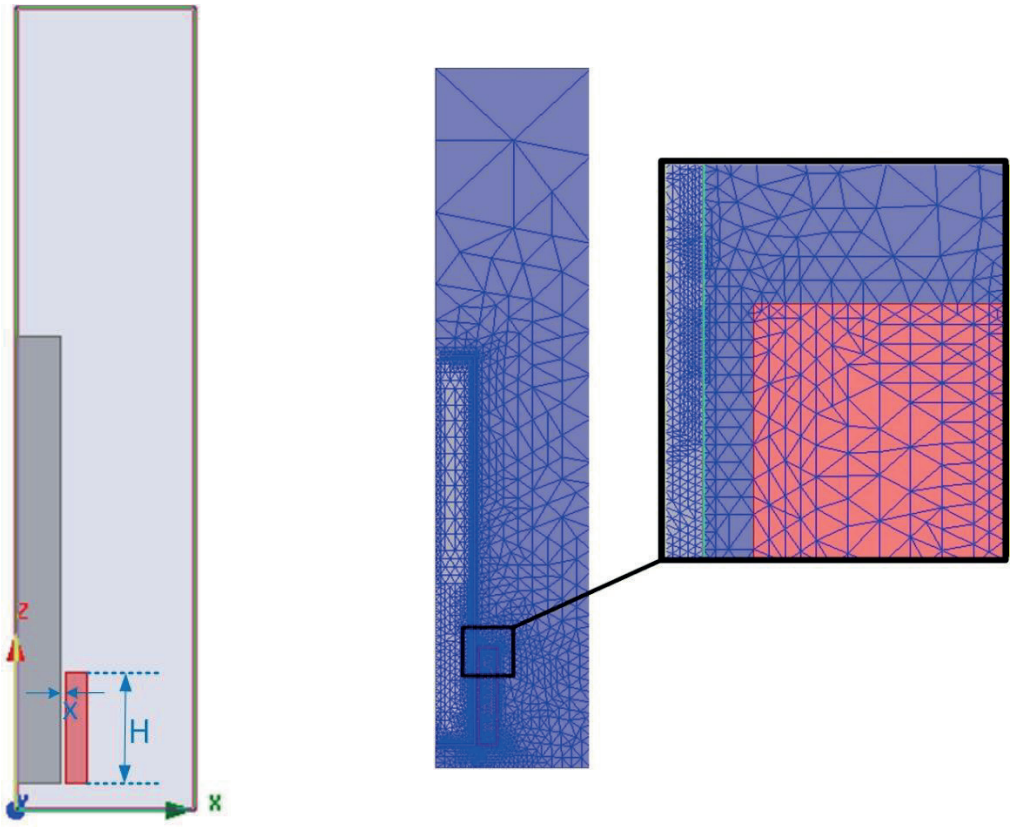

Figure 2. Model Geometry and Mesh Structure.

3. Analysis of Coil–Workpiece Distance and Coil Height

In this section, two fundamental geometric parameters that directly affect electromagnetic field distribution and the associated heat generation in induction heating systems—namely the coil–workpiece distance and the coil height—are examined. The analyses were carried out using the

finite element method, and the effects of both parameters on magnetic flux density, current density, and ohmic loss distributions were comparatively evaluated.

3.1. Effect of Coil-Workpiece Distance

The coil–workpiece distance (x) is one of the geometric parameters in induction heating systems that directly governs the interaction between the magnetic field generated by the coil and the workpiece. Variations in this distance have a decisive influence on magnetic field intensity, the induced eddy currents, and the resulting ohmic losses. Therefore, in this study, the coil–workpiece distance was systematically varied from 1 mm to 7 mm with a step size of 1 mm in order to examine the electromagnetic field distribution.

Figure 3 presents the magnetic flux density (Mag B) distributions on the workpiece for different coil–workpiece distances. At small distance values ($x \leq 2\,mm$), the magnetic coupling between the coil and the workpiece is strong, resulting in a high magnetic field intensity on the surface of the workpiece facing the coil. As the distance increases, the magnetic field intensity on the workpiece decreases. This behavior can be attributed to the attenuation of the magnetic field within the air gap.

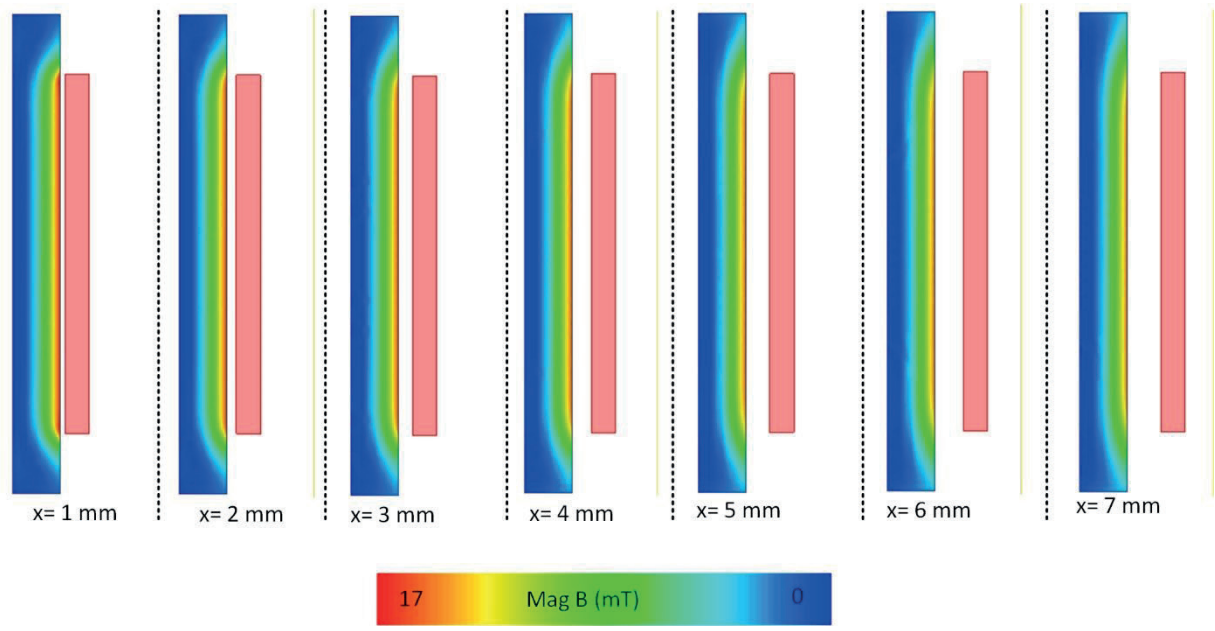

Figure 3. Variation of Mag B along the workpiece.

This variation in magnetic field distribution is consistent with the ohmic loss distributions shown in Figure 4. At small distance values, high ohmic loss densities are observed on the surface of the workpiece, indicating rapid and intense heat generation. Under constant excitation, as the distance increases, the ohmic loss decreases gradually, and a weakening of heat generation is observed. These results demonstrate that the coil–workpiece distance is a critical parameter governing heating power.

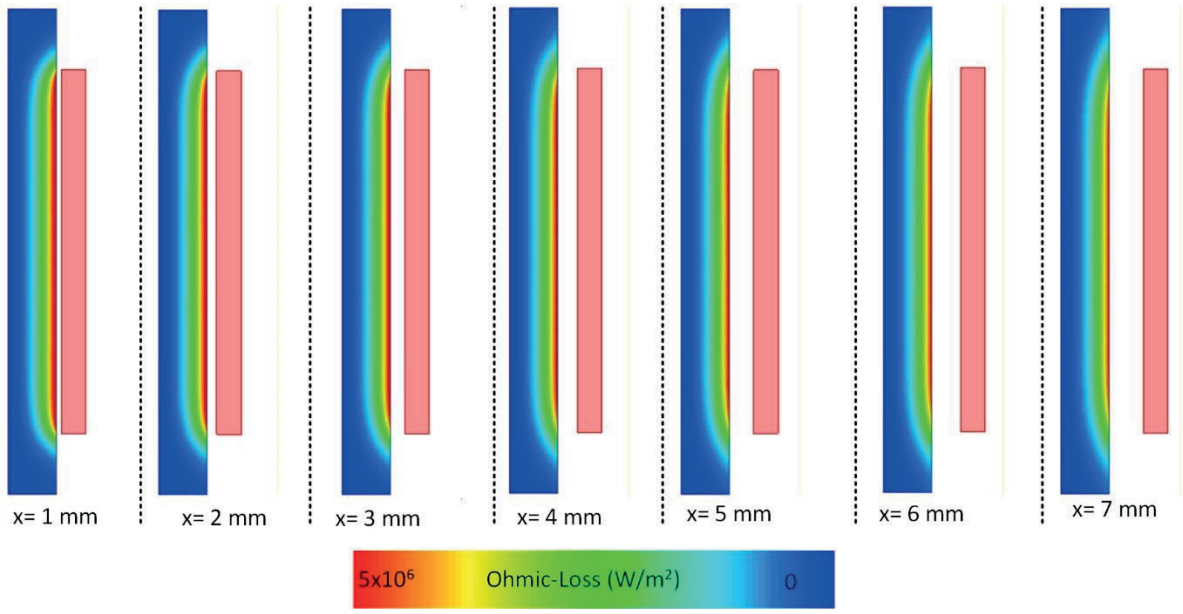

Figure 4. Effect of coil–workpiece distance on ohmic loss.

In the final analysis conducted in this section, a contour line was drawn along the workpiece in the direction facing the coil. The variation of magnetic flux density along this contour was obtained for different coil–workpiece distances and is presented in Figure 5.

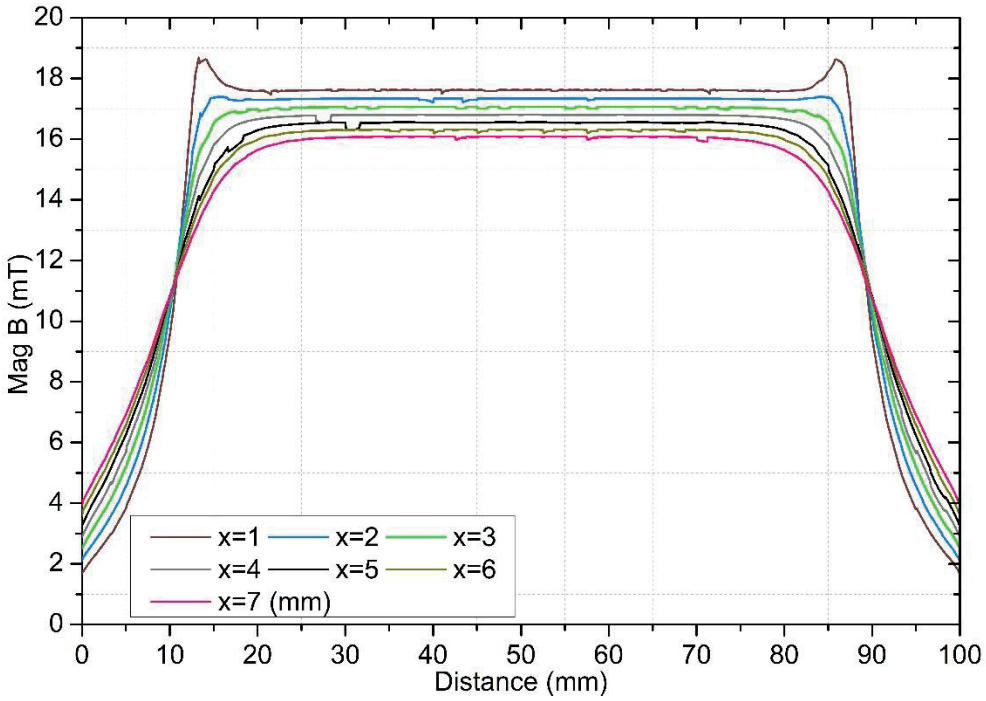

Figure 5. Variation of Mag B along the contour.

As the distance increases, the curves are clearly shifted downward along the entire axis, indicating a reduction in the average magnetic flux density. This behavior shows that the end

effect is present at all distance values; however, the overall heating level decreases as the distance increases.

When the obtained results are evaluated collectively, larger coil–workpiece distances lead to reduced heat generation due to weaker magnetic coupling, thereby requiring longer heating durations or higher supply current levels to reach the target temperature.

3.2.Influence of Coil Height on Induction Heating Performance

Coil height is one of the geometric parameters that determines the distribution of the magnetic field along the workpiece and, consequently, the homogeneity of heat generation in induction heating systems. In short coils, the concentration of the magnetic field within a limited region leads to dominant end effects, whereas increasing the coil height promotes a more balanced axial distribution of the magnetic field. In this study, the coil height was varied as H=25, 50, 75, 100, and 125 mm, while the workpiece geometry and the coil–workpiece distance were kept constant.

Figure 6 presents the magnetic flux density distributions obtained for different coil heights. For short coil lengths (H = 25 mm and 50 mm), the magnetic field is confined to the region occupied by the coil, resulting in low field levels over a large portion of the workpiece. This behavior leads to the concentration of the magnetic field in the end regions and the emergence of pronounced end effects. As the coil height increases, the magnetic field is observed to spread along the workpiece.

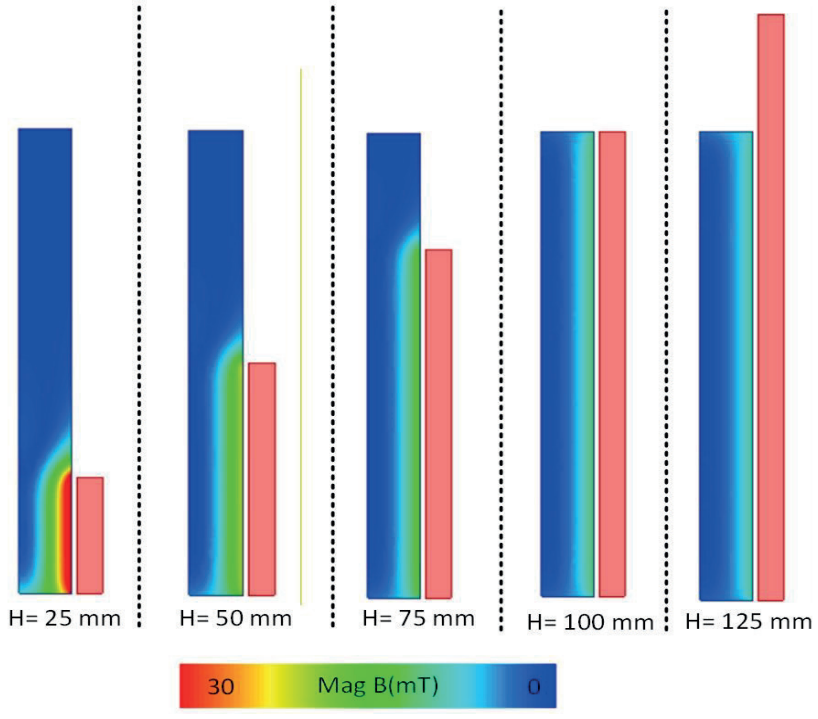

Figure 6. Magnetic flux density distribution.

The effect of coil height on the magnetic field distribution over the workpiece is illustrated in Figure 7 through the variation along a contour drawn on the surface of the workpiece facing the

coil. For short coils, the magnetic flux density reaches high values in the region overlapping with the coil, but decreases rapidly outside the coil boundaries. As the coil height increases, the Mag B curves clearly indicate a more homogeneous magnetic field distribution along the workpiece. In particular, when the coil height approaches the length of the workpiece, the magnetic field exhibits an almost uniform behavior.

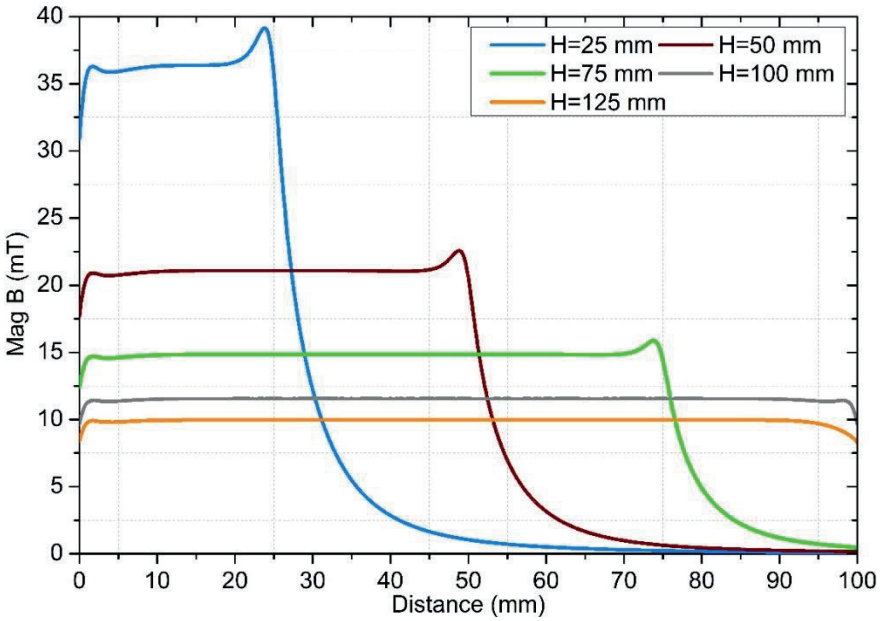

Figure 7. Variation of magnetic flux density along the contour.

This change in magnetic field distribution is directly correlated with the current density (J) vector distributions presented in Figure 8. For short coil lengths, the current density is concentrated in the limited region beneath the coil, whereas as the coil height increases, the current density spreads axially along the workpiece and becomes more uniform. This observation demonstrates that coil length directly influences the distribution of the induced eddy currents.

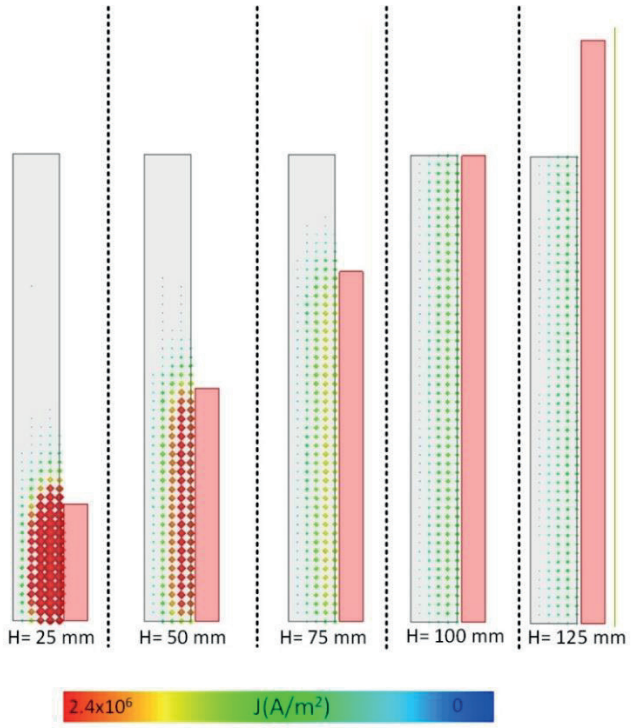

Figure 8. Variation of magnetic flux density along the contour.

Similarly, the ohmic loss distributions presented in Figure 9 clearly reveal the effect of coil height on heat generation. For short coils, ohmic losses are concentrated in specific regions, posing a risk of localized overheating, whereas increasing the coil height results in a more homogeneous distribution of ohmic losses. However, when the coil height is selected to be greater than the workpiece length, although homogeneity is maintained, the overall heat generation level decreases due to weakened electromagnetic coupling.

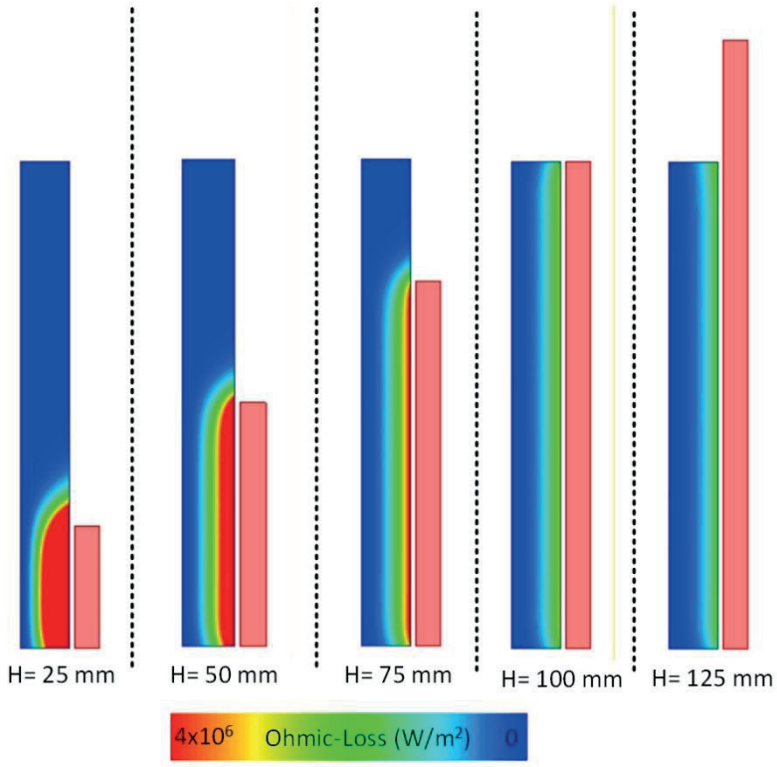

Figure 9. Variation of ohmic loss with coil length.

An evaluation of the obtained results clearly indicates that coil height has a significant influence on the homogeneity of heat distribution in induction heating systems. Selecting a coil height close to the workpiece length leads to the most balanced distributions of magnetic field, current density, and ohmic losses, whereas shorter coils are characterized by localized heating and longer coils by reduced heating intensity.

4. CONCLUSION

In this book chapter, the effects of two fundamental geometric parameters—namely the coil–workpiece distance and the coil height—which govern electromagnetic field distribution and the resulting heat generation in induction heating systems, were investigated using the finite element method. Within the scope of the study, magnetic flux density, current density, and ohmic loss distributions were obtained, thereby elucidating the decisive roles of both parameters in heating performance.

The analyses related to the coil–workpiece distance indicate that increasing the distance weakens the magnetic coupling, leading to a gradual reduction in magnetic flux density and ohmic losses. While high heating power is achieved at small distance values, a significant decrease in heat generation is observed as the distance increases, requiring longer heating durations or higher excitation levels to reach the target temperature. The results obtained for coil height demonstrate that this parameter primarily influences the homogeneity of heat distribution. For short coils, the magnetic field, current density, and ohmic losses are concentrated in specific regions, resulting in pronounced end effects; whereas increasing the coil height leads to a more balanced axial distribution of the electromagnetic field and a more homogeneous heat generation. When the coil height is selected close to the workpiece length, the magnetic field and ohmic loss distributions reach their most balanced configuration. Conversely, when the coil height exceeds the workpiece length, the overall heat generation level decreases due to weakened electromagnetic coupling, although homogeneity is preserved.

Overall, the obtained results clearly demonstrate that a trade-off exists between high heating rate and homogeneous heat distribution in induction heating systems. While the coil–workpiece distance emerges as the primary parameter governing heating intensity, the coil height is identified as the geometric variable controlling the homogeneity of heat generation.

References

Bao, L., Qi, X. W., Mei, R. B., Zhang, X., & Li, G. L. (2018). Investigation and modelling of work roll temperature in induction heating by finite element method. *Journal of the Southern African Institute of Mining and Metallurgy*, 118(7), 735-743.

Bertotti, G. (1998). Hysteresis in magnetism: for physicists, materials scientists, and engineers. *Academic press*.

Cui, P., Zhu, W., Ji, H., Chen, H., Hang, C., & Li, M. (2022). Analysis and optimization of induction heating processes by focusing the inner magnetism of the coil. *Applied Energy,* 321, 119316.

Cullity, B. D., & Graham, C. D. (2011). Introduction to magnetic materials. *John Wiley & Sons*.

Dalcalı, A., Özbay, H., & Öncü, S. (2020). The Effect of Working Frequency on Heating Depth in Induction Heating. *Journal of Engineering Sciences and Researches*, 2(1), 43-49.

Davies, E. J. (1990). Conduction and Induction Heating. *IEE Power Engineering Series*.

Du, H., Li, J., & Qu, Y. (2014). Mathematical Modeling of Eddy-Current Loss for a New Induction Heating Device. *Mathematical Problems in Engineering*, 2014(1), 923745.

Khazaal, M. H., Abdulbaqi, I. M., & Thejel R. H. (2016). Modeling, design and analysis of an induction heating coil for brazing process using FEM. *In 2016 Al-Sadeq International Conference on Multidisciplinary in IT and Communication Science and Applications*, 1-6.

Lucia, O., Maussion, P., Dede, E. J., & Burdío, J. M. (2014). Induction heating technology and its applications: past developments, current technology, and future challenges. *IEEE Transactions on Industrial Electronics*, 61(5), 2509-2520.

Lupi, S., Forzan, M., & Aliferov, A. (2014). Induction and Direct Resistance Heating Theory and Numerical Modeling. *Springer International Publishing AG*.

Park, H. S., & Dang, X. P. (2012). Optimization of the in-line induction heating process for hot forging in terms of saving operating energy. *International Journal of Precision Engineering and Manufacturing*, 13(7), 1085-1093.

Patidar, B., Hussain, M. M., Jha, S. K., Dikshit, B., & Sharma, A. (2018). Modelling and experimental demonstration of a litz coil-based high-temperature induction heating system for melting application. *IET Electric Power Applications*, 12(2), 161-168.

Patil, M., Choubey, R. K., & Jain, P. K. (2023). Influence of coil shapes on temperature distribution in induction heating process. *Materials Today: Proceedings*, 72, 3029-3035.

Patil, T. G., Patil, A. A., & Patil, V. H. (2014). A Critical review on different coil configurations used for induction heating system. *International Journal of Engineering, Business and Enterprise Applications*, 7(1), 35-39.

Rudnev, V., Loveless, D., Cook, R. L. (2017). Handbook of Induction Heating. *CRC Press*.

Sadeghipour, K., Dopkin, J. A., & Li, K. (1996). A computer aided finite element/experimental analysis of induction heating process of steel. *Computers in Industry*, 28(3), 195-205.

Sönmez, Ö. (2022). Investigation of Magnetic Induction Heating Using Finite Element Method. MSc Thesis, Akdeniz University.

Tavakoli, M. H., Karbaschi, H., & Samavat, F. (2011). Influence of workpiece height on the induction heating process. *Mathematical and Computer Modelling*, 54(1-2), 50-58.

Tavakoli, M. H., Ojaghi, A., Mohammadi-Manesh, E., & Mansour, M. (2009). Influence of coil geometry on the induction heating process in crystal growth systems. *Journal of Crystal Growth*, 311(6), 1594-1599.

Zhao, P., Zhao, L., Tan, L., Xu, Z., Wang, L., & Zhao, X. (2021). Investigation on the induction brazing of copper–steel tubes with different coil structures. *Welding in the World*, 65(6), 1181-1188.

Zinn, S., & Semiatin, S. L. (1988). Elements of Induction Heating: Design, Control, and Applications. *Asm International*.

Wang, K. F., Chandrasekar, S., & Yang, H. T. Y. (1992). Finite-element simulation of induction heat treatment. *Journal of Materials Engineering and Performance*, 1(1), 97-112.

CHAPTER 4

CHALLENGES AND REFORM STRATEGIES IN THE TURKISH ELECTRICITY SECTOR

Yelda KARATEPE MUMCU[1]

1 Assoc. Prof. Dr., Department of Electrical and Energy, Vocational School of Technical Sciences, Marmara University, Turkey. ORCID: https://orcid.org/0000-0001-9948-9413 email:ykaratepe@marmara.edu.tr

1. Introduction

Electricity is the backbone of modern economic and social infrastructure, functioning as a critical enabler of industrial development, public services, and daily life. In the context of developing economies, ensuring reliable, accessible, and sustainable electricity supply is both a technical and policy-driven challenge. Turkey, positioned at the crossroads of Europe and Asia, has undergone a significant transformation in its electricity sector over the past three decades. The transition from a state-controlled system to a liberalized market structure, initiated in the early 2000s, was driven by the need for improved efficiency, private sector participation, and alignment with EU energy directives [1].

Despite notable progress, Turkey's electricity sector still suffers from several chronic issues. Transmission and distribution losses remain substantially above OECD averages, with technical and non-technical losses accounting for nearly 10% of total electricity output as of 2022 [2]. Furthermore, regional disparities in service quality, frequent power outages, and pricing instability continue to affect both industrial productivity and household welfare [3].

Institutional reforms such as the establishment of EMRA (Energy Market Regulatory Authority) and the privatization of distribution networks have yielded mixed results. While market competition has improved, regulatory fragmentation and underinvestment in infrastructure persist [4]. Moreover, recent geopolitical tensions and supply chain shocks (e.g., post-COVID supply instability and the Ukraine crisis) have reignited debates around energy security and the resilience of the Turkish grid [5].

This chapter aims to provide a comprehensive overview of the structural evolution, persistent challenges, and reform trajectories in Turkey's electricity sector. Drawing upon recent empirical studies, energy policy reports, and regulatory evaluations, the discussion will center around four primary themes: (1) historical and institutional development, (2) transmission and service quality issues, (3) regulatory and market-based reforms, and (4) future pathways for sustainable electrification (Figure 1).

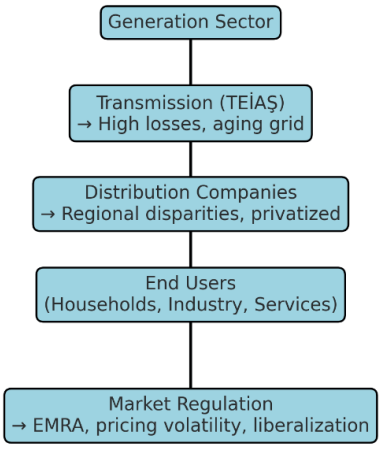

Figure 1. Structural Overview of the Turkish Electricity Sector and Key Reform Areas

2. Historical Development of the Electricity Sector in Turkey

The evolution of Turkey's electricity sector reflects a broader pattern seen in many developing economies, transitioning from a centralized, state-controlled model to a liberalized and partially privatized structure. The early phases of electrification in Turkey began during the late Ottoman era, with the first electricity generation facility established in 1914 in Istanbul by a foreign concessionaire. However, systematic national development began in the Republican period with the establishment of Etibank in 1935 and the General Directorate of Electrical Power Resources Survey and Development Administration (EIE) in 1935 [8].

Between the 1950s and 1980s, the state assumed a dominant role in electricity production and distribution. In 1970, the Turkish Electricity Authority (TEK) was established to consolidate generation, transmission, and distribution under a single public umbrella [9]. This model, though effective in expanding coverage, led to inefficiencies, bureaucratic delays, and insufficient investment in modern infrastructure.

In 1993, TEK was unbundled into two entities: TEAŞ (responsible for generation and transmission) and TEDAŞ (responsible for distribution) [7]. This structural separation marked the first concrete step toward a liberalized electricity market. The Electricity Market Law (No. 4628), enacted in 2001, was a turning point in Turkish energy policy, introducing market-based principles, competition, and the establishment of the Energy Market Regulatory Authority (EMRA), tasked with overseeing licensing, tariffs, and consumer protection [10].

By the mid-2000s, the privatization of distribution companies accelerated, transferring operational control to private entities under EMRA's regulation. The generation sector also saw increased private participation, especially after the enactment of the Electricity Market Law (No. 6446) in 2013, which refined licensing procedures and introduced mechanisms for market balancing and transparency [11].

Figure 2. Timeline of Major Institutional and Regulatory Milestones in the Turkish Electricity Sector [8-12]

TEİAŞ (Turkish Electricity Transmission Corporation), currently a state-owned enterprise, retains control over the transmission infrastructure and operates the balancing power market. TEDAŞ, although originally a public utility, has become more of a supervisory institution after the privatization of regional distribution companies [6]. This hybrid structure — centralized transmission and liberalized distribution — continues to evolve amidst growing electricity demand, climate commitments, and digital transformation (Figure 2).

Turkey's integration into the European electricity grid (ENTSO-E) in 2010 and the development of regional interconnections with neighbouring countries further underline the strategic and geopolitical importance of its energy infrastructure [12]. The historical trajectory reveals that while market liberalization brought improvements in efficiency and investment, it also introduced new challenges related to equity, regulatory oversight, and infrastructure quality.

3. Transmission and Service Quality Problems in the Turkish Electricity Sector

Despite significant regulatory reforms and increased private sector participation in Turkey's electricity market, transmission and distribution (T&D) problems remain key obstacles to achieving a fully efficient and equitable power system. Transmission infrastructure, largely operated by the state-owned TEİAŞ, suffers from aging equipment, capacity limitations in peak demand periods, and insufficient digital integration [13].

According to recent data, total electricity losses (technical + non-technical) in Turkey hover around 10%, nearly double the OECD average of 5–6% [14]. Technical losses arise from inadequate grid maintenance, outdated transformers, and insufficient monitoring technologies, particularly in rural and underdeveloped regions. Non-technical losses, such as electricity theft and unregistered usage, are more prevalent in the southeastern provinces, where enforcement mechanisms are weak [15].

Service quality issues are reflected in both the System Average Interruption Duration Index (SAIDI) and the System Average Interruption Frequency Index (SAIFI) — key international benchmarks of distribution reliability. In 2021, the average SAIDI for Turkey was 356 minutes per customer per year, significantly above EU standards, which typically range between 50–100 minutes [16]. These figures point to systemic underperformance, especially among certain distribution companies operating in economically disadvantaged regions.

Privatization of distribution networks, while improving financial discipline and investment in some areas, has not uniformly translated into service quality improvements. According to a comparative study by Erdinç & Öztürk (2022), customer complaints regarding voltage instability and unexpected outages have increased in regions where investment lagged post-privatization [17].

Moreover, regulatory asymmetry and inconsistent oversight by EMRA have allowed some operators to underperform without meaningful penalties. In several audit reports, it was found that despite failing service metrics, companies were allowed tariff hikes or cost recovery adjustments, undermining consumer trust and distorting competition [18].

Another concern is the lack of smart grid infrastructure across the country. While pilot projects have been initiated in major cities like Istanbul and Ankara, large-scale implementation of real-time monitoring, automated fault detection, and demand-side management remains limited

[19]. These technological gaps exacerbate response times during blackouts and reduce resilience in the face of natural disasters or cyberattacks.

In summary, the Turkish electricity sector's transmission and distribution performance continues to be constrained by infrastructural aging, uneven investment, regulatory shortfalls, and limited technological modernization. Addressing these challenges is essential not only for service reliability but also for achieving energy equity and long-term sustainability in the sector.

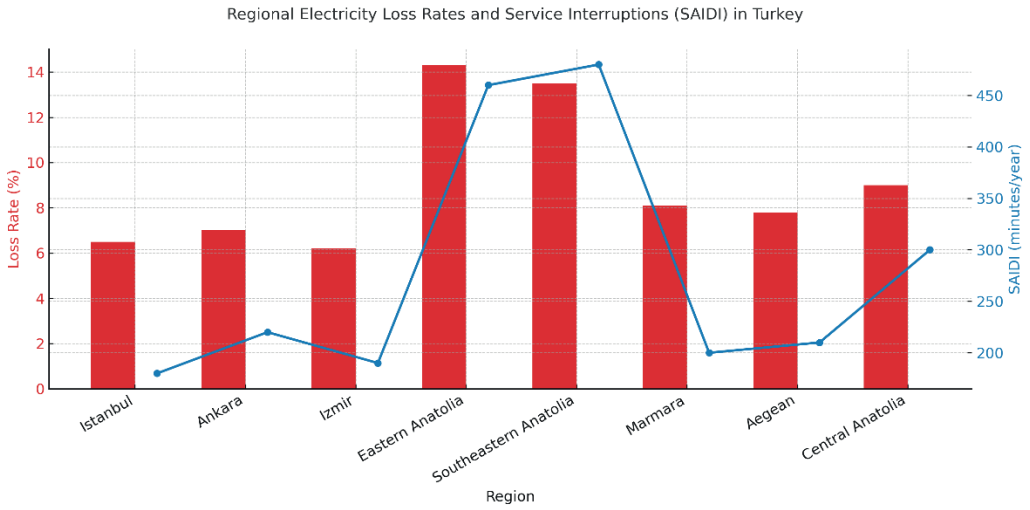

Figure 3. Regional Distribution of Electricity Loss Rates and SAIDI Values in Turkey [13-17].

4. Regulatory Challenges and Market Reform Outcomes in the Turkish Electricity Sector

Turkey's electricity market reforms—initiated in the early 2000s and deepened by the 2013 Electricity Market Law (No. 6446)—aimed to liberalize generation and distribution, encourage private investment, and align with EU internal energy market principles. The Energy Market Regulatory Authority (EMRA) was established to oversee licensing, tariff regulation, market balancing, and consumer protection. Despite these developments, key regulatory and structural challenges persist that limit the full realization of reform objectives [20].

One of the primary issues is regulatory asymmetry between public and private actors. While private distribution companies operate under revenue-cap models, the state-owned TEİAŞ (transmission) and public hydropower generators are not subject to the same market-based performance pressures. This imbalance creates market distortions that inhibit fair competition and reduce incentives for efficiency improvements [21].

Another concern lies in regulatory fragmentation and policy volatility**.** Several studies highlight that frequent tariff formula changes, inconsistent cost pass-through mechanisms, and ad hoc regulatory interventions have created uncertainty, discouraging long-term investments in the sector—particularly in renewables and smart grid infrastructure [22].

In terms of market structure, Turkey's liberalization reforms succeeded in attracting considerable private capital into generation and distribution. By 2023, over 75% of electricity generation capacity was operated by the private sector, a sharp contrast to the pre-2001 era [23].

However, this transition also led to increased market concentration, where vertically integrated firms gained excessive control over both generation and retail supply. The Herfindahl-Hirschman Index (HHI) scores for generation markets remain above EU competition thresholds, especially in hydro and gas segments [24].

Furthermore, regulatory enforcement by EMRA has been inconsistent. While the institution is legally independent, it remains vulnerable to political influence, especially in tariff decisions and licensing for politically sensitive projects. As observed by Aydın and Şahin (2021), penalties for non-compliance are often delayed or diluted, reducing the deterrent power of regulation [25].

Another critical limitation is consumer engagement and transparency. Despite formal liberalization, most residential consumers are not active market participants. The eligibility threshold for switching suppliers remains high, and public awareness about competitive tariffs is low. This undermines retail market development and places excessive focus on regulated pricing mechanisms [26].

Lastly, energy poverty and affordability concerns have constrained EMRA's ability to apply full cost-reflective pricing. Political resistance to tariff hikes—especially during elections or inflation surges—has led to regulatory capture, where economic decisions are subordinated to short-term political goals [27].

In conclusion, Turkey's electricity market reform has made notable progress in liberalization and infrastructure expansion. However, the regulatory landscape remains fragmented, and performance outcomes are hindered by political interference, asymmetric oversight, and market concentration. Future regulatory reforms must prioritize independence, transparency, and consumer empowerment to ensure equitable and sustainable energy governance.

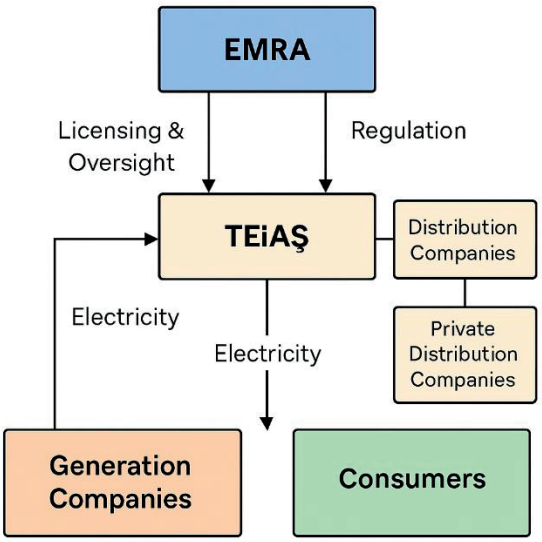

Figure 4. Institutional Framework of the Turkish Electricity Market and Regulatory Flows [20-27].

5. Renewable Energy and Integration Challenges in the Turkish Electricity Sector

Turkey has made remarkable progress in expanding renewable energy capacity, particularly in wind, solar, and hydroelectric power. As of 2023, renewables account for over 52% of installed electricity generation capacity, driven by policy tools such as feed-in tariffs (YEKDEM), licensing incentives, and public-private partnerships [28]. However, integrating these sources effectively into the national grid has introduced a new set of technical, regulatory, and economic challenges (Figure 5).

Figure 5. Operational Flow of Turkey's Renewable Energy Feed-in Tariff Mechanism (YEKDEM) [28-33]

A central issue is the limited flexibility of the transmission system, managed by TEİAŞ. The grid, originally designed for centralized thermal generation, struggles to accommodate the variable nature of wind and solar power. As a result, regions with high renewable penetration—such as Aegean and Central Anatolia—have experienced curtailment**,** where power from wind or solar plants is not dispatched due to grid congestion or voltage instability [29].

Additionally, grid connection delays and capacity limitations hinder investor confidence. Although TEİAŞ has published Regional Connection Capacities (RCCs) to manage expectations, actual implementation lags behind due to bureaucratic hurdles and limited digitalization of network planning tools [30].

Turkey's electricity market also lacks an advanced balancing mechanism for variable renewables. Unlike more mature markets, intraday and ancillary services are not sufficiently dynamic to react to short-term supply-demand mismatches caused by renewables. This has led to increased imbalance costs for producers and system operators alike [31].

Another challenge is the geographical mismatch between renewable resource potential and demand centers. While southeastern Anatolia and inner Aegean regions have vast solar and wind potential, major demand hubs like Istanbul, Izmir, and Ankara are located elsewhere.

Without sufficient interregional transmission capacity, this mismatch limits the economic value of renewables [32] (Figüre 6).

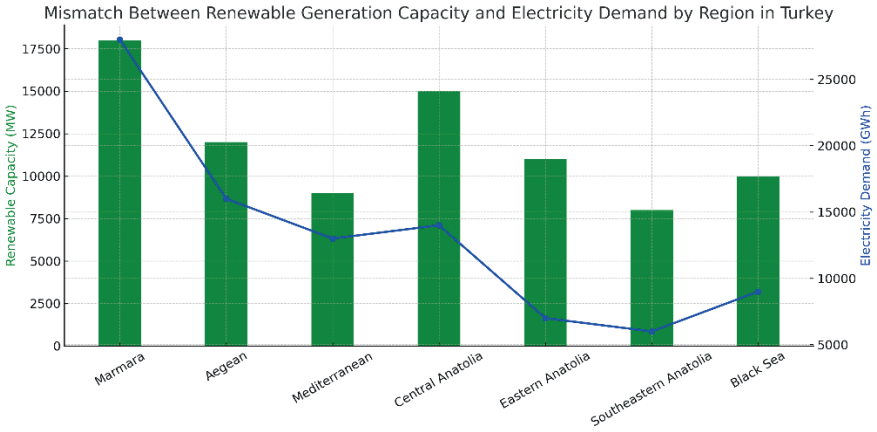

Figure 6. Regional Mismatch Between Renewable Capacity and Electricity Demand in Turkey [28-32]

From a regulatory perspective, EMRA has made improvements in streamlining licensing and updating grid codes. Yet, policy uncertainty, such as abrupt changes to feed-in tariff schemes and localization requirements, continues to erode investor trust. For example, changes introduced in 2021 to the YEKDEM system altered foreign currency guarantees and limited incentive durations, which many analysts argue reduced foreign direct investment in renewables [33].

Moreover, distributed generation (DG)—especially rooftop solar—remains underdeveloped due to unclear net metering policies and a lack of standardized application processes for residential and commercial users. This limits bottom-up participation in the energy transition and centralizes control in large-scale renewable developers [34].

In conclusion, Turkey's renewable energy expansion is commendable, but effective integration requires urgent action on transmission upgrades, market design reforms, and stable regulatory frameworks. Without these, the country risks underutilizing its renewable potential and missing its decarbonization targets under the Paris Agreement.

6. Affordability, Energy Poverty, and Consumer Protection in Turkey's Electricity Sector

Ensuring electricity affordability and addressing energy poverty have emerged as central challenges in Turkey's energy policy landscape, particularly in the aftermath of the COVID-19 pandemic and global energy price shocks. Although Turkey's electricity market underwent significant liberalization, the government maintains price controls for residential consumers, especially through cross-subsidization mechanisms and targeted tariffs [35].

According to EMRA data, as of 2023, the average household electricity price in Turkey was around $0.07/kWh—below the EU average—but still burdensome for low-income households, particularly in the eastern and southeastern regions [36]. The energy burden, defined as the

share of household income spent on electricity, exceeds 10% for nearly 20% of Turkish households, indicating moderate to severe energy poverty [37].

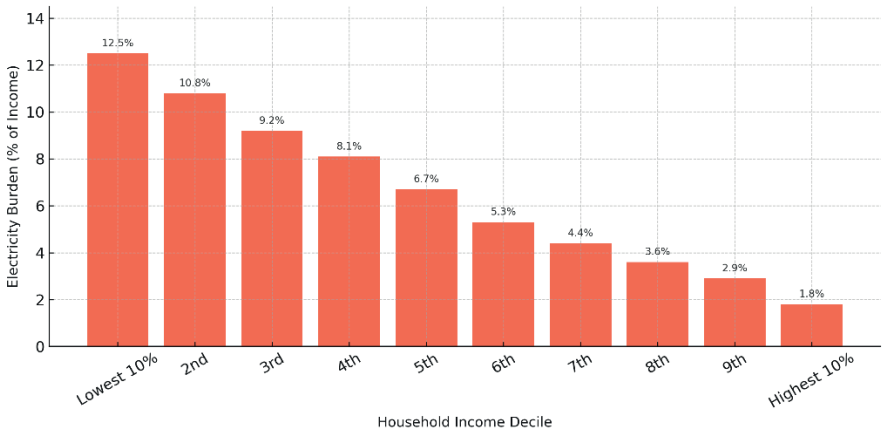

Figure 7. Electricity Burden by Household Income Decile in Turkey [35, 37, 38].

To mitigate this, the government introduced electricity bill support programs, where eligible low-income households receive monthly subsidies (ranging from 75–150 kWh/month depending on family size). However, studies indicate that the program's targeting efficiency is limited due to outdated social registry data and administrative fragmentation [38].

Furthermore, cross-subsidies—where industrial and commercial users pay more to keep residential tariffs low—have distorted market signals and reduced competitiveness in energy-intensive industries. These distortions are compounded by political interference in tariff-setting processes, especially during election cycles or periods of inflation volatility [39].

EMRA has also expanded consumer protection regulations, including mandatory disclosure of unit prices, standard billing formats, and complaint resolution protocols. Nevertheless, public awareness of consumer rights remains low, particularly among rural and elderly populations [40].

From a long-term perspective, energy poverty is expected to persist unless structural reforms address underlying income disparities, regional inequalities in infrastructure, and the lack of efficiency in housing stock. Studies also emphasize the need to align affordability with climate goals, especially in light of the Just Transition framework under the EU Green Deal [41].

In conclusion, while Turkey has taken important steps to support vulnerable electricity consumers, current policies remain fragmented, reactive, and insufficiently targeted. A comprehensive national strategy for energy affordability—integrating income support, energy efficiency, and progressive tariff design—is urgently needed.

7. Environmental and Climate Considerations in Turkey's Electricity Sector

Turkey's electricity sector is at the center of the country's climate and environmental policy challenges. Despite increasing renewable capacity, coal-fired generation continues to contribute significantly to greenhouse gas (GHG) emissions. In 2022, electricity generation was responsible for nearly 34% of Turkey's total CO_2 emissions, largely driven by domestic lignite and imported coal [42] (Figure 8).

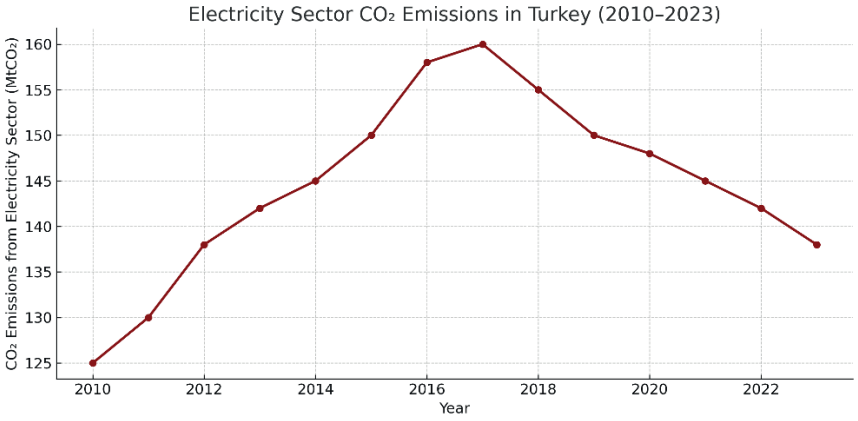

Figure 8. Electricity Sector CO_2 Emissions in Turkey (2010–2023).

The country's delayed ratification of the Paris Agreement (approved only in 2021) and absence of an official net-zero target until 2053 have contributed to international criticism. Although Turkey has committed to reducing emissions by 41% below business-as-usual by 2030, analysts note that these targets remain unaligned with the EU's more aggressive Green Deal framework [43].

One major issue is the lack of a national carbon pricing mechanism**.** Unlike the EU Emissions Trading Scheme (ETS), Turkey does not yet have a functioning carbon market. While there are ongoing feasibility studies, the absence of carbon pricing has led to continued investment in coal and gas, creating a lock-in effect on fossil infrastructure [44].

Environmental externalities are further amplified by outdated coal plants that lack modern flue gas treatment systems. Reports by the Ministry of Environment show that at least 6 major thermal plants failed to meet EU environmental standards as of 2023 [45].

There are also significant land-use and biodiversity impacts associated with large-scale hydro and solar installations. Hydropower plants in Eastern Anatolia have altered river ecosystems and displaced local communities, while solar farms in Central Anatolia have raised concerns about habitat loss and water stress in arid zones [46].

Turkey's National Energy and Climate Plan (NECP) is still under development, with draft versions emphasizing energy efficiency, grid modernization, and renewable incentives. However, policy inconsistency, overlapping mandates between ministries, and lack of legally binding climate targets undermine implementation [47].

Another concern is climate resilience of the electricity infrastructure. Rising summer temperatures and prolonged droughts have reduced hydroelectric generation reliability and increased grid stress during peak cooling demand. Yet, few investments have been made in climate-proofing the grid through storage, digital monitoring, or heat-resilient transmission systems [48].

To meet climate goals, researchers emphasize that Turkey must urgently phase out coal, introduce carbon pricing, accelerate offshore wind deployment, and integrate climate risk into electricity planning. Without such measures, the electricity sector will remain misaligned with both national and international climate commitments.

9. Grid Modernization and Digitalization Efforts in Turkey

Turkey's electricity grid modernization efforts have accelerated over the past decade in response to increasing integration of renewables, demand-side complexities, and global trends in digitalization. Institutions such as TEİAŞ (transmission operator), TEDAŞ (distribution), and EMRA have each introduced digital transformation projects with varying levels of progress [49].

Key components of modernization include:

- SCADA and remote terminal unit (RTU) upgrades across high-voltage substations
- Geographic Information Systems (GIS) integration for asset management
- Advanced Metering Infrastructure (AMI) and Automated Meter Reading (AMR) systems to enable dynamic pricing and consumption transparency [50]

Despite these initiatives, a fully integrated Smart Grid ecosystem remains in early stages. A 2023 study revealed that while 85% of TEİAŞ transmission infrastructure is SCADA-enabled, only 40% of regional distribution operators have completed AMR rollouts [51].

Cybersecurity has emerged as a growing concern. As digital control expands, threats to critical energy infrastructure have increased. EMRA has initiated a Grid Cybersecurity Framework, including mandatory audits and encryption standards for digital substations and control centers [52].

Another challenge is data integration across multiple platforms and agencies. Lack of standardization in digital platforms and overlapping software systems hinders real-time responsiveness and decision-making. Pilot projects for interoperability—especially between EMRA and TEİAŞ databases—have shown early promise but face institutional resistance and budget constraints [53].

Furthermore, there is a significant skills and capacity gap in digital grid management. University–industry collaborations are still limited, and most SCADA/AMI deployments rely on foreign technology vendors, raising concerns about knowledge transfer and long-term independence [54].

Looking forward, experts stress the need for:

- A national smart grid strategy with enforceable targets
- Investment in digital grid resilience (e.g., against climate-induced heat stress)

- Capacity-building programs for grid engineers and IT specialists
- Clearer coordination among TEİAŞ, TEDAŞ, and EMRA

Turkey's modernization journey is advancing—but remains fragmented and underfunded. If aligned with long-term decarbonization and electrification goals, grid digitalization can be a key enabler of a more efficient, flexible, and secure power system.

10. Conclusion and Strategic Outlook

Turkey's electricity sector stands at a critical juncture—between the legacy of state-centric governance and the demands of a decentralized, decarbonized, and digitalized future. Over the past three decades, the country has made significant strides in liberalization, capacity expansion, and regulatory reform. Yet, persistent challenges continue to compromise efficiency, equity, and sustainability.

This chapter’s multi-dimensional analysis reveals several intertwined issues:

- **Institutional Fragmentation** undermines strategic coherence across transmission, distribution, regulation, and policy planning.
- **Grid Vulnerability**—manifesting in high losses, service quality gaps, and weak climate resilience—limits reliability and consumer confidence.
- **Regulatory Asymmetry** and market concentration distort competition and hinder the realization of efficiency gains.
- **Renewable Integration Barriers**, both technical and procedural, risk underutilizing Turkey’s vast clean energy potential.
- **Affordability and Energy Poverty**, exacerbated by economic instability, require stronger social protection mechanisms and data-driven targeting.
- **Climate and Environmental Misalignment**, especially with continued coal reliance and absence of a carbon pricing system, pose long-term systemic risks.
- **Digital Transformation**, though underway, remains fragmented, underfunded, and heavily dependent on foreign technological know-how.

Strategic Recommendations for a Just and Resilient Energy Transition

To navigate these challenges and seize emerging opportunities, Turkey must embrace a bold, strategic, and inclusive energy vision:

1. **Recalibrate Governance**
   Establish a centralized energy policy coordination mechanism to align EMRA, TEİAŞ, TEDAŞ, and the Ministry under a shared strategic vision.
2. **Invest in Grid Modernization**
   Expand SCADA/AMI coverage, digital monitoring, and climate-resilient infrastructure, especially in underserved regions.
3. **Foster Market Transparency and Competition**
   Address market concentration, revise eligibility thresholds for supplier switching, and empower consumers through data access and tariff literacy.
4. **Advance Renewable Grid Integration**
   Accelerate transmission upgrades, reform balancing markets, and localize renewable project approvals to reduce curtailment and improve dispatchability.

5. **Implement Comprehensive Affordability Policies**
   Move beyond cross-subsidies by integrating income-based support, efficiency retrofits, and progressive tariff models.
6. **Integrate Climate Targets into Energy Planning**
   Introduce carbon pricing mechanisms, phase out coal, and embed resilience and biodiversity safeguards into project evaluation.
7. **Build Domestic Digital and Human Capacity**
   Prioritize local R&D in smart grid solutions, establish interdisciplinary training programs, and create incentives for domestic technology providers.

The future of Turkey's electricity sector depends not only on megawatts added or kilometers of grid laid, but on institutional vision, societal consensus, and political will. A successful transition requires balancing market efficiency with social justice, energy security with environmental stewardship, and innovation with public accountability.

By embedding long-term thinking, transparency, and resilience into electricity sector governance, Turkey can not only meet its domestic development needs, but also position itself as a regional leader in sustainable energy transformation.

References

[1] Yeldan, E., et al. (2019). *Structural Reforms in Turkey's Energy Markets: Liberalization and Its Discontents*. Energy Policy, 128, 147-155. https://doi.org/10.1016/j.enpol.2018.12.032

[2] IEA (2023). *Turkey Energy Profile – Electricity Market Overview*. International Energy Agency. https://www.iea.org/reports/turkey-energy-profile

[3] Aydın, N. (2022). *Regional Disparities in Electricity Service Quality in Turkey: Causes and Consequences*. Renewable and Sustainable Energy Reviews, 158, 112064. https://doi.org/10.1016/j.rser.2022.112064

[4] Kabakçı, A., & Biresselioğlu, M. E. (2021). *Evaluation of Electricity Distribution Reforms in Turkey: A Political Economy Perspective*. Energy Policy, 156, 112404. https://doi.org/10.1016/j.enpol.2021.112404

[5] Bilgen, S. (2022). *Energy Security in Turkey: The Role of Geopolitical and Pandemic Shocks*. Energy Reports, 8, 1284–1295. https://doi.org/10.1016/j.egyr.2022.03.043

[6] EPDK (2021). *Electricity Market Annual Report*. Energy Market Regulatory Authority. https://www.epdk.gov.tr

[7] World Bank (2020). *Turkey Energy Sector Note: Challenges and Opportunities*. https://www.worldbank.org/en/country/turkey

[8] EIE (2010). *History of Electricity in Turkey*. General Directorate of Electrical Power Resources.

[9] Altun, M. (2016). *The Evolution of Turkey's Electricity Market: Liberalization and Structural Changes*. Energy Policy, 98, 324-332. https://doi.org/10.1016/j.enpol.2016.08.016

[10] EMRA (2020). *Legal Framework of the Turkish Electricity Market*. Energy Market Regulatory Authority.

[11] Duman, T. (2019). *Electricity Market Reform in Turkey: An Assessment of Liberalization Outcomes*. Energy Reports, 5, 1205–1214. https://doi.org/10.1016/j.egyr.2019.08.017

[12] Bilgin, M. (2018). *Turkey's Energy Diplomacy and Electricity Interconnectivity with Europe*. Energy Policy, 120, 500–510. https://doi.org/10.1016/j.enpol.2018.05.036

[13] IEA (2023). *Turkey Electricity System Profile – Grid Infrastructure Overview*. International Energy Agency. https://www.iea.org

[14] EMRA (2022). *Loss and Leakage Statistics by Region*. Energy Market Regulatory Authority. https://www.epdk.gov.tr

[15] Atalay, Y., & Aydın, G. (2020). *Electricity Theft and Losses in Turkish Distribution Networks: Regional Patterns and Countermeasures*. Energy Policy, 142, 111481. https://doi.org/10.1016/j.enpol.2020.111481

[16] ERRA (2022). *Electricity Distribution Benchmarking Report: Turkey Profile*. Energy Regulators Regional Association. https://erranet.org

[17] Erdinç, M., & Öztürk, S. (2022). *Post-Privatization Performance in Turkey's Electricity Distribution Sector: Evidence from SAIDI and SAIFI Metrics*. Utilities Policy, 78, 101429. https://doi.org/10.1016/j.jup.2022.101429

[18] EPDK (2021). *Audit Reports on Electricity Distribution Companies*. Energy Market Regulatory Authority. https://www.epdk.gov.tr

[19] Bilgen, S. (2021). *Smart Grid Development in Turkey: Opportunities and Barriers*. Renewable and Sustainable Energy Reviews, 145, 111123. https://doi.org/10.101/10.1016/j.rser.2021.111123

[20] Duman, T. (2023). *Asymmetric Regulation and Competition in the Turkish Electricity Market*. Energy Policy, 179, 113548. https://doi.org/10.1016/j.enpol.2023.113548

[21] EMRA (2023). *Electricity Market Development Report*. Energy Market Regulatory Authority. https://www.epdk.gov.tr

[22] Aydın, M., & Şahin, S. (2021). *Regulatory Enforcement Gaps in Liberalized Electricity Markets: A Turkish Case Study*. Utilities Policy, 72, 101238. https://doi.org/10.1016/j.jup.2021.101238

[23] World Bank (2022). *Turkey: Assessment of Electricity Market Outcomes and Policy Options*. https://www.worldbank.org

[24] Arslan, H., & Dicle, M. F. (2022). *Market Concentration and Competition Risks in Turkish Power Generation*. Energy Economics, 110, 106012. https://doi.org/10.1016/j.eneco.2022.106012

[25] Bilgen, S. (2020). *Energy Policy and Regulatory Capture in Turkey's Electricity Sector*. Energy Research & Social Science, 69, 101737. https://doi.org/10.1016/j.erss.2020.101737

[26] Erdoğan, N. (2023). *Retail Market Barriers in the Turkish Electricity Sector: Regulatory and Consumer Perspectives*. Renewable and Sustainable Energy Reviews, 175, 113143. https://doi.org/10.1016/j.rser.2023.113143

[27] EMRA (2022). *Tariff and Consumer Protection Report*. Energy Market Regulatory Authority. https://www.epdk.gov.tr

[28] EMRA (2023). Electricity Market Indicators – Renewable Capacity. Energy Market Regulatory Authority. https://www.epdk.gov.tr

[29] Bilgen, S., & Kaygusuz, K. (2022). Curtailment and Grid Integration Barriers for Renewables in Turkey. Energy Policy, 163, 112885. https://doi.org/10.1016/j.enpol.2022.112885

[30] TEİAŞ (2022). Regional Grid Connection Capacity Reports. Turkish Electricity Transmission Corporation. https://www.teias.gov.tr

[31] Aydın, G., & Korkmaz, A. (2021). Balancing Mechanisms and Renewable Variability in Turkey's Power Market. Energy Reports, 7, 3883–3894. https://doi.org/10.1016/j.egyr.2021.06.047

[32] Kılkış, Ş., et al. (2020). Spatial Mismatch Between Renewable Supply and Electricity Demand in Turkey. Renewable Energy, 161, 879–891. https://doi.org/10.1016/j.renene.2020.07.094

[33] Eroğlu, H. (2021). Uncertainty in Renewable Energy Support Schemes: The Case of Turkey's YEKDEM Transition. Renewable and Sustainable Energy Reviews, 143, 110911. https://doi.org/10.1016/j.rser.2021.110911

[34] Aksoy, M., & Koç, M. (2023). Barriers to Distributed Solar Adoption in Turkey. Sustainable Energy Technologies and Assessments, 54, 102982. https://doi.org/10.1016/j.seta.2022.102982

[35] Çelik, K., & Arslan, H. (2022). Electricity Affordability and Cross-Subsidies in Turkey: Policy Trade-Offs. Energy Policy, 168, 113075. https://doi.org/10.1016/j.enpol.2022.113075

[36] EMRA (2023). Retail Electricity Tariff Statistics. Energy Market Regulatory Authority. https://www.epdk.gov.tr

[37] OECD (2022). Measuring Energy Poverty in Turkey: Income and Burden Approaches. https://www.oecd.org

[38] Korkmaz, S., & Aydın, G. (2021). Effectiveness of Electricity Subsidies in Reducing Energy Poverty: Evidence from Turkey. Utilities Policy, 70, 101222. https://doi.org/10.1016/j.jup.2021.101222

[39] World Bank (2022). Turkey Energy Sector Public Expenditure Review. https://www.worldbank.org

[40] ERRA (2023). Consumer Protection and Electricity Market Transparency: Turkey Country Profile. https://erranet.org

[41] Bilgen, S. (2023). Energy Justice and the Green Transition: Turkey's Position Under the EU Climate Policy. Renewable and Sustainable Energy Reviews, 177, 113245. https://doi.org/10.1016/j.rser.2023.113245

[42] IEA (2023). Turkey Energy Profile: Electricity and Emissions Overview. International Energy Agency. https://www.iea.org

[43] Aksoy, M., & Bilgen, S. (2022). Paris Agreement Commitments and the Turkish Power Sector. Energy Reports, 8, 3468–3477. https://doi.org/10.1016/j.egyr.2022.02.124

[44] Çoban, S., & Güneş, E. (2023). Feasibility of Carbon Pricing in Turkey: ETS and Beyond. Energy Policy, 179, 113512. https://doi.org/10.1016/j.enpol.2023.113512

[45] Ministry of Environment (2023). Thermal Power Plant Emissions and Compliance Report. Republic of Turkey. https://csb.gov.tr

[46] Kılkış, Ş., & Ayaz, A. (2021). Renewable Energy vs. Biodiversity Trade-offs in Turkey. Renewable and Sustainable Energy Reviews, 147, 111233. https://doi.org/10.1016/j.rser.2021.111233

[47] EBRD (2023). Draft National Energy and Climate Plan – Turkey Overview. European Bank for Reconstruction and Development. https://www.ebrd.com

[48] Güven, G., & Demirtaş, E. (2022). Climate Resilience of the Turkish Electricity Grid: Current Gaps and Future Needs. Energy and Climate Journal, 14(3), 224–235. https://doi.org/10.1016/j.egy.2022.03.008

[49] Keskin, M. (2021). Smart Grids and Turkey: Overview of the Current Power System. Uppsala University.

[50] Uğuz, M. (2024). A Quantitative Analysis on Smart Grid Transformation in Turkey. Middle East Technical University.

[51] Yumak, K. et al. (2018). Turkey's Smart Grid Roadmap for Electrical Distribution Systems in Vision 2035. IEEE. https://ieeexplore.ieee.org/document/8571730

[52] EMRA (2023). Grid Cybersecurity Guidelines and Technical Reports. https://www.epdk.gov.tr

[53] Gürbüz, K.P. (2019). Smart Grid Applications in Turkish Distribution Systems. METU Graduate School. PDF

[54] EBRD (2023). Turkey Digitalization Diagnostic in Energy Infrastructure. https://www.ebrd.com

CHAPTER 5

PID CONTROLLER TUNING METHODS FOR DC MOTOR CONTROL: CLASSICAL AND METAHEURISTIC APPROACHES

Ahmet TOP[1]

1 Dr. Öğr. Üyesi, Department of Electrical and Electronics Engineering, Faculty of Technology, Fırat University, Turkey, ORCID ID: http://orcid.org/0000-0001-6672-2119

INTRODUCTION

DC (direct current) motors operate directly from a DC power source and are capable of converting electrical energy into mechanical energy. There are many types, such as brushless DC (BLDC) motors [1], servo motors [2], stepper motors [3], and brushed DC motors [4], and they are reasonably priced when compared to AC motors [5]. Furthermore, DC motors may be controlled using extremely straightforward and reliable techniques. quick efficiency and quick beginning torque in abrupt load rises are further benefits. Nevertheless, brushless DC motors have become a viable alternative to DC motors, which are inadequate in several ways, including the need for routine maintenance, rapid mechanical deterioration of the output, acoustic noise, glare, and the impact of brushes on efficiency. Because of its benefits, which include silent operation, quick dynamic response, strong torque characteristics, and efficient operation, brushless DC motors are favored [6].

DC motors have become quite widespread today and have become an important necessity to assist human activities. For instance, they are frequently employed in industrial settings [7], operating a conveyor machine to move an object [8], drawing water from underground to the surface using a water pump [9], cooling a room by turning a fan [10], robotics [11], and electric vehicles [12], etc. As a result, controlling the motor's speed is crucial with a suitable control algorithm to stabilize the speed of the motor, especially under variable and nonlinear loads and under the influence of disturbing inputs [13].

Some controllers, such as PI (proportional, integral) Controller [14], PID (PI+derivative) Controller [15], ANFIS-Based Hybrid P-I-D Controller [16], Fractional Sequence PID [17], Fuzzy Logic Controller [18], Model Reference Adaptive Control (MRAC) [19], and Integral State Feedback [20] have been applied to DC motor systems. The best-known of these is the PID [21]. Some of the advantages of PID are simple structure, good stability, strong resistance, and ease of implementation in software or hardware [22]. It is applied in many systems such as temperature control [23], aircraft systems [24], and transport robots [25]. Parameter tuning is the primary issue that is commonly discussed in PID [26]. Put differently, to achieve the best possible system performance, the parameter values of the Proportionality Constant (Kp), Integral Constant (Ki), and Derivative Constant (Kd) are determined[27].

Among the methods employed for this is classical methods such as Ziegler-Nichols, gain-phase margin, and Cohen-Coon methods. However, these methods require knowledge of mathematical models and are difficult to tune the parameters; therefore, It takes a long time to find parameters, control accuracy is not good, and the parameters used are not optimal. Therefore, in recent years, researchers have used many optimization algorithms such as Teaching learning based optimization [28], Artificial Bee Colony Algorithm [29], Grey Wolf Optimization [30], Firefly Algorithm [31], Differential Evolution [32], Genetic Algorithm [33], Sine Cosine Algorithm [34], Water Wave Optimization [35] for tuning PID parameters.

In the studies in the literature mentioned above, researchers have proposed PID controllers with different approaches to improve transient characteristics such as DC motor speed response, overshoot percentage, settling time, rise time, peak value, and steady-state error. Furthermore, since no algorithm can guarantee finding the best parameter values for a controller designed for DC motor speed control, researchers have opted for algorithms with different approaches.

This section presents classical methods and some metaheuristic optimization methods used for parameter tuning of PID controllers in speed and position control of DC motors.

2. MODELING OF DC MOTOR

DC motors are categorized as externally stimulated and self-excited types. Since externally excited DC motors are generally used for speed adjustment and position control, the modeling of the DC motor whose equivalent circuit is given in Figure 1 is presented in this section [36]. The transfer function is created according to speed control.

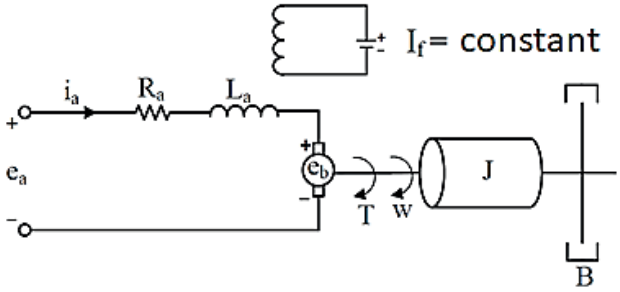

Figure 1. A DC motor speed control system's equivalent circuit.

As demonstrated by the DC motor's equivalent circuit shown in Figure 1, e_a represents the applied armature voltage (V), i_a represents the armature current (A), R_a represents the armature resistance (Ω), L_a represents the armature inductance (H), i_f represents the field current (A), e_b represents the back electromotive force (V), T represents the motor torque (N.m), w represents the angular velocity of the motor shaft (rad/s), J represents the moment of inertia of the motor (kg.m^2), K represents the motor torque constant (N.m/A), K_b represents the electromotor force constant (V.s/rad), B represents the motor friction constant (N.m.s/rad) and T_L represents the load moment (N.m) [37].

The induced voltage is linearly proportional to the angular velocity when the flux is constant, where $\frac{d\theta}{dt} = w(t)$. Accordingly, the voltage e_b is given in Equation 1.

$$e_b = K_b \frac{d\theta}{dt} = K_b w(t) \tag{1}$$

An armature-controlled DC servo motor's speed is determined by the armature voltage e_a. Consequently, Equation 2 provides the differential equation for the armature circuit of the DC motor.

$$e_a(t) = L_a \frac{di_a(t)}{dt} + R_a i_a + e_b(t) \tag{2}$$

When the load moment is considered as zero, the moment (T) corresponding to the sum of the moments of inertia and friction, and whose equation is given in Equation 3, is directly proportional to the armature current.

$$T(t) = J \frac{dw(t)}{dt} + Bw(t) = Ki_a(t) \tag{3}$$

When all initial conditions in Equations 1-3 are taken as zero, and the Laplace transform is applied, the transfer function of the uncontrolled DC motor for zero load moment ($T_L(s)$) is obtained as in Equation 7, following Equations 4-6.

$$E_b(s) = K_b w(s) \tag{4}$$

$$E_a(s) = (L_a s + R_a) I_a + E_b(s) \tag{5}$$

$$T(s) = (Js + B) w(s) = K I_a(s) \tag{6}$$

$$\frac{w(s)}{E_a(s)} = \frac{K}{(L_a s + R_a)(Js + B) + K_b K} \tag{7}$$

When the applied armature voltage is taken as zero, Equation 8 describes the relationship between motor speed and load torque.

$$\frac{w(s)}{T_L(s)} = \frac{(L_a s + R_a)}{(L_a s + R_a)(Js + B) + K_b K} \tag{8}$$

Figure 2 shows DC motor system's block diagram. The armature, motor torque constant, mechanical component, and electromotive force constant are the parts of a DC motor, as illustrated in Figure 2.

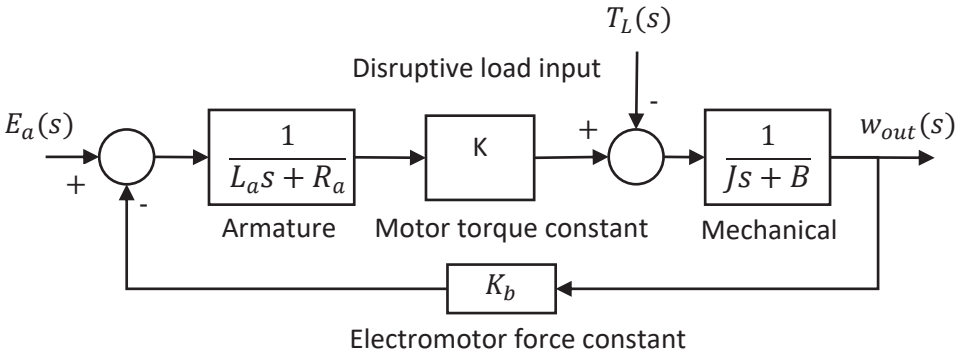

Figure 2. Uncontrolled DC motor's block diagram.

3. PID Control

PID, controller is frequently used to regulate a DC motor's speed [38]. Basically, the concept of a PID controller is a simple three-term controller used to increase stability and reduce steady-state error [39]. For many control issues, PID control provides the most effective and straightforward solution, encompassing both transient and steady-state responses.

Proportional Term: An output value proportionate to the current error value is produced by the proportional term [40]. By multiplying the error by a constant Kp, the proportional response can be modified. The proportionate term can be found using:

$$P_{out} = K_p * Error \tag{9}$$

In response to a given change in error, a high Kp results in a significant change in output. The system may become unstable if the proportionate gain is excessively high. On the other hand, a little gain leads to a less sensitive or responsive controller and a weak output reaction to a significant input mistake. When reacting to system disturbances, the control action may be insufficient if the Kp is too low. The proportional term should account for most of the output variance, according to tuning theory and industrial application [41].

Integral Term: The integral term's contribution [40] is proportionate to the error's magnitude and duration. The integral term contribution provides the accumulated deviation that must be adjusted beforehand by adding the instantaneous mistake over time. The integral gain (Ki) is then multiplied by the total error. Equation 10 represents the integral output.

$$I_{out} = K_i * \int Error\,.dt \tag{10}$$

Differential Term: The derivative of the process error can be obtained by calculating the slope of the error with respect to time and multiplying this rate of change by the derivative gain Kd. [40]. The derivative gain, Kd, is the amount that the derivative term contributes to the total control action. The following is the derivative term:

$$D_{out} = K_d * \frac{d}{dt}(Error) \tag{11}$$

The PID's transfer function is usually written using the "gain notation" given by equation 11 or the "time constant notation" given by equation 12.

$$\mathrm{T(s)} = \mathrm{K_p} + \mathrm{K_i}\frac{1}{\mathrm{s}} + \mathrm{K_d s} \tag{11}$$

$$\mathrm{T(s)} = \mathrm{K_p}(1 + \frac{1}{\mathrm{T_i s}} + \mathrm{T_d s}) \tag{12}$$

Here, T_i is the integral time constant, and T_d is the derivative time constant. The general block diagram for this control method is given in Figure 3.

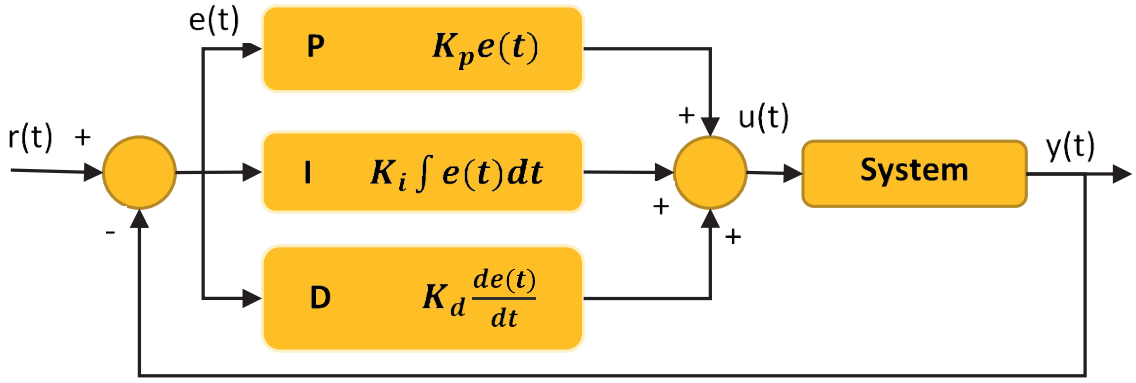

Figure 3. PID control block diagram.

Studies conducted to determine PID control parameters are examined in two separate categories. In the first category, the control parameters are fixed throughout the operating time, and at the end of the time, the parameters are adjusted offline or optimally selected according to the controller output. In the second category, the control parameters are calculated automatically through the automatic tuning method used and applied to the system. Since the analytical calculation of the ideal PID parameters for the controller in the system is quite difficult, especially in complex systems, automatic tuning methods have been developed to overcome this problem. P-I-D parameters are adjusted according to the desired response from the system [42].

3.1 Traditional techniques for adjusting PID parameters

Classical methods attempt to tune controllers by examining and revealing system characteristics, either analytically or with the help of graphical methods. Such tuning strategies aim to obtain controller configurations for common models. To calculate the dynamics of these systems, the step response of the systems is obtained [43]. Different classical techniques were developed as a result of the different equations that characterize this reaction. Since the gains of the controllers depend on the transfer function variables, it is essential to establish the configuration using conventional methods before adjusting the PID parameters. Despite the widespread usage of traditional PID tuning techniques, their behavior frequently deviates from the intended goal or objective [44]. Below is a description of a few of these techniques.

3.1.1. Ziegler-Nichols Method

In this approach, one of the most preferred gain-parameter tuning methods, was developed in 1942 by John G. Ziegler and Nathaniel B. Nichols. The Ziegler-Nichols method is designed as a closed control loop. While finding the appropriate gain parameters for the system, the Ki (integral) and Kd (derivative) coefficients are set to zero. The Kp, is increased starting from 0 until a continuous, non-damped, and non-unstable oscillation is observed at the system output. The gain value at which the desired oscillation is captured is called Ku, and the oscillation period is called Tu. Using the Ku and Tu parameters, the Kp, Ki, and Kd values are found to suit the system. Table 1 gives the equations that allow reaching the PID gain parameters according to the Ku and Tu values. Although it is an old technique, its tendency to lead the system to instability is a significant disadvantage [42].

Table 1. Calculation of PID gain parameters [45]

	K_p	T_i	T_d
P	$0.5K_U$		
PI	$0.4K_U$	$0.8T_U$	
PID	$0.6K_U$	$0.5T_U$	$0.125T_U$

3.1.2. Cohen-Coon Tuning Method

In this tuning method, the step response curve of the system is first obtained. The time when the system output reaches 28.3% of its steady-state value (t1) and when it reaches 63.2% (t2) is determined [46]. With these values, ζm = (3/2)(t2 - t1), d = t2 - ζm, and the ratio of the system output to its steady-state value, i.e., its gain, $K_m = \frac{yss(t)}{r(t)}$ are calculated. Then, the PID parameters are calculated using Table 2 [47].

Table 2. Cohen-Coon PID parameter tuning rules

Controller	K_p	T_i	T_d
P	$\frac{\zeta m}{K_m}(1+\frac{d}{3\zeta m})$	-	-
PI	$\frac{\zeta m}{K_m d}(\frac{9}{10}+\frac{d}{12\zeta m})$	$d\frac{30+3d/\zeta m}{9+20d/\zeta m}$	-
PD	$\frac{\zeta m}{K_m d}(\frac{5}{4}+\frac{d}{12\zeta m})$	-	$d\frac{6-2d/\zeta m}{22+3d/\zeta m}$
PID	$\frac{\zeta m}{K_m d}(\frac{4}{3}+\frac{d}{4\zeta m})$	$d\frac{32+6d/\zeta m}{13+8d/\zeta m}$	$d\frac{4}{11+2d/\zeta m}$

3.1.3. Chien-Hrones-Reswick (CHR) Tuning Method

In this method, PID parameters are obtained by utilizing the open-loop step response of the system. Rules showing the calculation of parameters using L (dead time), T (time constant), K (gain) and a=KL/T are given in Table 3 for reference regulation and in Table 4 for stopping the disturbance effect [48].

Table 3. Rules for tuning PID parameters with the CHR method (reference regulation)

Controller	With a 0% overage			With a 20% overage		
	Kp	Ti	Td	Kp	Ti	Td
P	0,3/a	-	-	0,7/a	-	-
PI	0,35/a	1,2T	-	0,6/a	T	-
PID	0,6/a	T	0,5L	0,95/a	1,4T	0,47L

Table 4. Rules for tuning PID parameters using the CHR method (stopping the disturbance effect)

Controller	With a 0% overage			With a 20% overage		
	Kp	Ti	Td	Kp	Ti	Td
P	0,3/a	-	-	0,7/a	-	-
PI	0,6/a	4L	-	0,7/a	2,3L	-
PID	0,95/a	2,4L	0,42L	1,2/a	2L	0,42L

3.2. Optimization methods of PID parameters tuning

Optimization is needed in areas such as control engineering, mechanics, networks, economics, production, planning, marketing, transportation, etc. Optimization is the effort to find the best solution for a problem, within the given constraints, if any. There are two types of optimization problems: single-objective and multi-objective. In single-objective optimization problems, the comparison of the solutions reached is carried out by comparing the objective or cost function values corresponding to the solutions. A better solution produces a better fitness value. In multi-objective optimization problems, the goodness of the solution reached is related to its dominance. Dominance is a fundamental concept for Multi-Objective Optimization. If a solution is better than another solution for at least one of the given objectives, and produces the same or better results for the other objectives, then the solution in question is said to be dominant over the other solution [49]. When PID controllers are tuned with optimization approaches, it is possible to achieve controller gains that rise as quickly as possible, produce low overshoot, and near-zero steady-state error responses. Optimization approaches used for this purpose are generally metaheuristic optimization algorithms [50].

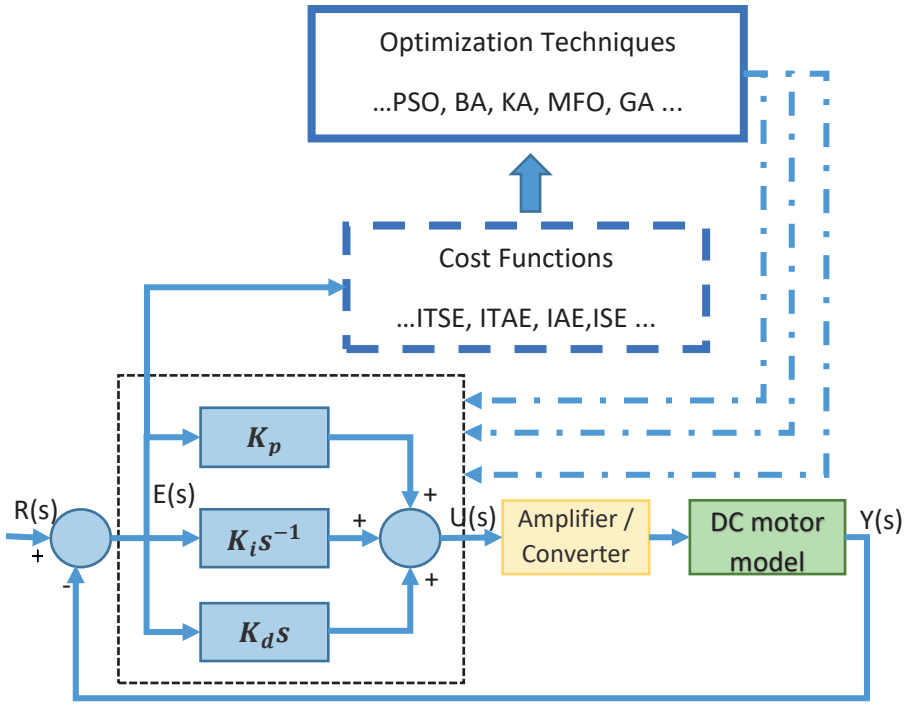

Figure 4. Conceptual design of PID controller optimization for DC.

Strategies based on metaheuristics solve issues by offering nearly ideal answers in a reasonable amount of time. Due to their efficiency and effectiveness in solving large and complex problems, the use of metaheuristic techniques has grown significantly in recent years. Metaheuristic methods are a type of heuristic method that performs better than simple heuristic methods. Meta means "beyond" or "higher level". Each metaheuristic algorithm uses a specific mixture of local and global search. Different results are usually obtained through randomization. Regardless of whether metaheuristic methods are accepted or not, there is no standard or verifiable definition for heuristic methods and metaheuristic methods in the literature. Many academics and researchers use heuristic methods and metaheuristic methods interchangeably. This evaluation will also adopt the same rule [51]. The block diagram for the PID tuning with optimization performed for the DC motor model is shown in Figure 4.

When evaluating the efficiency of a PID controller, a number of performance metrics are applied in optimization techniques to measure error dynamics and time-accumulated error. Among these, the most prominent are the integral of absolute error (IAE), ITAE, integral of squared error (ISE), and integral of time squared error (ITSE), which are standard in measuring controller performance. These metrics are critical for distinguishing the response of a control system in various operational scenarios and determining the most suitable control approach. The equations of these performance metrics are stated in Equations 13-16 [6].

$$ISE = \int_0^\infty e^2(t)dt \tag{13}$$

$$IAE = \int_0^\infty |e(t)|dt \tag{14}$$

$$ITSE = \int_0^\infty te^2(t)dt \tag{15}$$

$$ITAE = \int_0^\infty t|e(t)|dt \tag{16}$$

where $e(t)$ represents the difference between the controlled variable and the set point, and t is the time. Below are some examples from the literature where optimization algorithms, belonging to the class of metaheuristic algorithms in DC motor control, are used for parameter tuning in PID controllers.

3.2.1. Particle Swarm Optimization (PSO)

A swarm-based optimization system called particle swarm optimization was created by simulating fish and bird social behavior. Eberhart and Kennedy created it in 1995 [52].

The PSO algorithm's general working logic is as follows: A random distribution is used to create the particles' starting placements in the first stage. The positions' fitness values are computed in the second step. These fitness values are obtained using the fitness function. In the third stage, each particle's optimal location ($p_{best,i}$) and the swarm's best position thus far (g_{best}) are ascertained for the pertinent iteration. This decision is based on the fitness values determined in the second stage. Each particle's position and velocity are updated in the fourth stage using $p_{best,i}$ and g_{best}. The velocity is updated using a weighting coefficient (inertia weight). The algorithm moves on to the second stage after storing the optimal answer from these updates in memory at the fifth stage. Until the halting requirement is satisfied, this iterative process keeps going. The velocity and position update formulae are shown in Equations 17 and 18.

$$v_{t+1} = wv_t + c_1r_1(p_{best} - p_t) + c_2r_2(g_{best} - p_t) \tag{17}$$

$$p_{t+1} = p_t + v_{t+1} \tag{18}$$

Here $v_{t+1}$is the current velocity of the particle, w is the inertial weight, $v_t$is the old velocity of the particle, r_1, r_2 are random numbers generated in the interval (0,1), c_1, c_2 are the learning coefficients, p_t is the old position of the particle, p_{t+1} is the new position of the particle [53].

3.2.2.Sine Cosine Algorithm (SCA)

Mirjalili offered a recently created population-based metaheuristic optimization method called SCA. It mimics the behavior of mathematical sine and cosine functions [54]. Many SCA versions, including USMN-SCA [55], MTV-SCA [56], and others, have been thoroughly researched and used in DC motor control [54], renewable energy systems [57], and buck converter [58] optimizations in recent years. Equation 19 illustrates how the sine or cosine function is used to update solutions.

$$R_i^{t+1} = \begin{cases} R_i^t + r_1.\sin(r_2).|r_3.Y_i^t - R_i^t|, & r_4 < 5 \\ R_i^t + r_1.\cos(r_2).|r_3.Y_i^t - R_i^t|, & r_4 \geq 5 \end{cases} \tag{19}$$

In this case, t stands for the current iteration, R_i for the current solution location, and Y_i for the goal solution. The region of the subsequent solution is determined by the transformation parameter, or r_1. Equation 20 adaptively modifies the range of the sine and cosine functions in Equation 19.

$$r_1 = b.\left(1 - \frac{t}{T}\right) \tag{20}$$

where b>0 is a constant, T is the total number of iterations, and t is the current iteration. The following solution's movement direction (i.e., either towards or away from Y_i) is determined by the random variable $r_2 \in [0,2\pi]$ in Equation 9. Furthermore, r_3 offers random weights as a stochastic factor to either raise (r_3>1) or decrease (r_3<1) Y_i's influence on defining the distance. Equation 19 uses the term r_4 to alternate between the sine and cosine functions [54]. This technique uses the time-weighted absolute error as a fitness function to guarantee correct comparison with PSO.

3.2.3. Whale Optimization Algorithm

This algorithm, proposed by Mirjalili and Lewis in 2016, was created inspired by the unique hunting method of humpback whales [59]. Humpback whales gather their prey together with large and interconnected bubble nets. As humpback whales rise to the surface of the water within the bubble nets, they approach their prey by breathing in and out. As they get closer to their prey, they gradually narrow the bubble net circle, making their target smaller. It is known that they use this method to find their prey, immobilize their prey, or hide themselves from their prey. In the whale optimization algorithm, mathematical equations were created according to this hunting method. The relevant equations are given in Equations 21-24.

$$D = |CX^*(t) - X(t)| \tag{21}$$

$$X(t+1) = X^*(t) - AD \tag{22}$$

Looking at the equations in equations 21 and 22, A and C are constant vectors, X* is the best solution that is repeated at the end of each iteration, and t is the number of iterations. The calculations of the constant vectors A and C are given in equations 23 and 24, respectively.

$$A = 2ar - a \tag{23}$$

$$C = 2r \tag{24}$$

Here, 'r' is a random vector between [0,1] and 'a' is a vector that declines linearly from 2 to 0 throughout the iteration. The following describes how the whale optimization algorithm is implemented:

Step 1: Initialize the positions of humpback whales in the algorithm randomly after defining the population size, lower bound, upper bound, number of iterations, and number of variables.

Step 2: Calculate the objective function for each humpback whale using the predefined objective function.

Step 3: Find the objective function for the best humpback whale.

Step 4: Update the positions of the humpback whales.

Step 5: Until the stopping requirement is satisfied, increase the number of iterations and repeat the steps, going back to Step 2.

Step 6: Return the best humpback whale position corresponding to the best objective function.

3.2.4. Moth-Flame Optimization (MFO)

The moth-flame optimization algorithm (MFO) was developed by Mirjalili in 2015 and is based on the transverse orientation mechanism of moth navigation found in nature [60]. Equations 25–29 provide the mathematical formulas developed using this navigation technique in the moth-flame optimization process. In a d-dimensional space, the quantity of moths is regarded as search agents in flight. These moths begin in an arbitrary location. The matrix M contains the moths' locations in each dimension. Equation 25 makes clear that n stands for the number of moths and d for the number of dimensions, or variables.

$$M = \begin{pmatrix} m_{1.1} & \dots & m_{1,d} \\ \vdots & \ddots & \vdots \\ m_{n,1} & \dots & m_{n,d} \end{pmatrix} \tag{25}$$

The objective function of each trust is stored in the OM sequence specified in equation 26, where n is the number of trusts.

$$OM = \begin{bmatrix} OM_1 \\ OM_2 \\ \vdots \\ OM_n \end{bmatrix} \tag{26}$$

The flames are represented by the F matrix given in Equation 27, which also keeps track of each moth's best position to date. When a moth discovers a better solution, the flames are likewise updated. Only one of the flames can be used by each moth to update its position. It is evident from Equations 25 and 27 that the sizes of the F and M matrices are equal. Additionally, n is the number of moths and d is the number of variables in Equation 27.

$$F = \begin{pmatrix} F_{1.1} & \dots & F_{1,d} \\ \vdots & \ddots & \vdots \\ F_{n,1} & \dots & F_{n,d} \end{pmatrix} \tag{27}$$

The OF array takes the objective function values of the solutions stored in the flame matrix.

$$OF = \begin{bmatrix} OF_1 \\ OF_2 \\ \vdots \\ OF_n \end{bmatrix} \tag{28}$$

In the equation given in Equation 28, the positions of the moths are updated based on the logarithmic spiral function.

$$S(M_i, F_j) = D_i, e^b \cos(2\pi t) + F_j \tag{29}$$

In Equation 29, D_i is the separation between the j-th flame and the i-th moth., t is a random number chosen between [-1,1], and b is a constant number specifying the shape of the logarithmic spiral. The implementation of moth flame optimization is described as follows:

Step 1: After defining the population size, lower bound, upper bound, number of iterations, and number of variables, randomly initialize the positions of the moths in the algorithm.

Step 2: Calculate the objective function for each moth using the previously defined objective function.

Step 3: Find the best moth objective function.

Step 4: Adjust the moths' locations.

Step 5: Until the stopping criteria has been fulfilled, increase the number of iterations and repeat the steps, going back to Step 2.

3.2.5. Kidney-Inspired Algorithm

Kidneys are vital organs in the urinary system of human biological structure, with crucial functions such as filtering blood by removing excess water and waste through urine and regulating the amount of ions in the blood. Therefore, they are responsible for blood chemistry, fluid balance, and consequently the overall health of the human body. The kidney process is a repetitive process that can be summarized in four steps: filtration, reabsorption, secretion, and excretion. Filtration begins in the glomerular capillaries, where solutes are transferred to the tubules under both Bowman's capsule pressure and blood pressure. Then, reabsorption is applied to return useful substances from the tubules back to the bloodstream. The movement of solutes towards the renal tubules is secretion. The final process is excretion, where excess substances (water, waste, and ions) are removed from the urine [61]. The kidney-inspired algorithm (KI) was first proposed by Jaddi et al. (2017) [62,63]. In the initial stage of KA, as in other population-based algorithms, an arbitrary population of possible solutes is generated and their objective functions are calculated. Each solute can be considered as water particles and substances dissolved in plasma in the biological kidney system. In each iteration, a new solute is created for each of the solutes, moving towards the best solute obtained so far. The movement of a solute in this algorithm is formulated as follows [62]:

$$S_{i+1} = S_i + rand(S_{best} - S_i) \tag{30}$$

In this case, rand is a randomly chosen number between zero and a specified number, S represents a solute in the population, Si represents a solute in the i-th iteration, and Sbest represents the best solute found thus far in earlier iterations. By applying the filtering operator, the solutes in the population with higher quality are transferred to the filtered blood (FB), while the remaining solutes are transferred to the waste (W). This is accomplished by using a filtering rate that is computed and modified in each KA cycle. The filtration rate (f_r) is similar to the glomerular filtration rate in the biological kidney system and is calculated as follows [62]:

$$fr = \alpha \sum_{i}^{p} f(x_i)/p \tag{31}$$

In this case, p is the population size, In the interval [0,1], α is a constant number, and $f(x_i)$ is the solute x's objective function in the i-th iteration. A solute's acceptance as a member of FB or W is determined by the following rule: if the solute's quality is higher than fr, it is accepted as a member of FB; if not, it is accepted as a member of W. If a solute is placed in W, the reabsorption operator gives the solute another chance to improve itself and become part of FB. This can only happen if the solute meets the filtering ratio after the re-application of the motion operator in Equation 30. This is similar to the reabsorption of useful particles into the

bloodstream in the biological kidney system. If this chance cannot be seized, the solute is expelled from W, and another random solute is added to W in its place. Furthermore, after the filtration process, if a solute placed in the FB is better than the worst solute in the FB, then the worst solute is secreted (removed) from the FB. However, if this solute is not better than the worst solute in the FB, then the solute itself is secreted. This is similar to the secretion of harmful particles in the bloodstream in the biological kidney system. After that, the solutes in the FB are sorted to update the best solute obtained so far. Finally, FB and W are combined to create a new population, and the filtration rate is updated. The addition of random solutes can be thought of as the continuous addition of water and solutes to the glomerular capillaries in the biological kidney system [61].

3.2.6. Bee Algorithm

The Bee Algorithm is an optimization method inspired by nature and developed by modeling the foraging behavior of bees. First developed by Pham et al., the Bee Algorithm is a swarm intelligence-based scanning algorithm that mimics the resource (nectar, water, etc.) foraging behavior of honey bees [64].

During optimization, a number of the Bee Algorithm's parameters must be changed. The number of optimal scanning zones chosen from n visited points (m), the number of explorer bees (n), the number of bees sent to the best e scanning zones (nep), the number of elite scanning zones within the chosen m scanning zones (e), how many bees were sent to the remaining (m-e) scanning zones (nsp), the size of the scanning zone (ngh), and the number of iterations taken into consideration as the stopping criterion (itr). The optimization problem begins with randomly sending n explorer bees into the scanning space. In the second step, the suitability of the points scanned by the scout bees is evaluated. In the third step, m scan regions with more suitable values are selected from among n scan regions. In the fourth and fifth steps, the elite scan regions (e) with the best suitability values and the remaining scan regions (m-e) are selected from the m scan regions. The neighborhood scan dimension (ngh) is determined for these regions. For neighborhood scanning in the selected scan regions, a more detailed search is performed by dispatching additional follower bees (nep) to the best scan region (e), which has more promising solutions, and fewer follower bees (nsp) to the other scan regions compared to the other selected scan regions. Within each scan region, the bee with the best value is chosen. All bees are eliminated from the scan space in the sixth, seventh, and eighth phases, with the exception of the bee whose value is best for each scan region. The remaining bees (n-m) in the swarm are randomly sent back into the scan space to obtain new potential solutions. The process continues until the optimization halting criterion (itr) is met. After each iteration, the new swarm; It consists of representatives of each selected scanning area and scout bees that perform random scanning [65].

3.2.7. Genetic Algorithm

In nature, living organisms transmit certain physical and biological characteristics or abilities acquired throughout their lifespans to the next generation through genes. As a result, every generation surpasses earlier generations in the sense of adaptation to its living environment. During the creation of new individuals, genes taken from two random individuals (considered a male and a female) combine to create a new genetic structure and a new individual. The new individual contains a random mixture of the characteristics of the individuals that created it. This mixture results from the cross-breeding process during the combination of genes. An individual with negative characteristics cannot survive in nature and will eventually die out. This is called natural selection. An individual with positive characteristics survives and, in the process, undergoes changes and acquires new characteristics; this is called mutation. These self-

improving individuals reproduce again, transmitting both the positive characteristics inherited from their ancestors and the newly acquired positive characteristics to the next generation. Thus, the generation continues to exist by improving itself and reproducing. This cycle continues as long as living things survive. Inspired by this cycle, J. Holland and Goldberg created the genetic algorithm in 1975 [66]. Figure 5 shows the genetic algorithm's general block diagram. First, fitness values are examined, and a random beginning population is generated. The process is completed if a gene in the population offers the solution; if not, genetic operators are used to construct a new population and recalculate fitness values. Until a workable solution is discovered, this process is repeated [67].

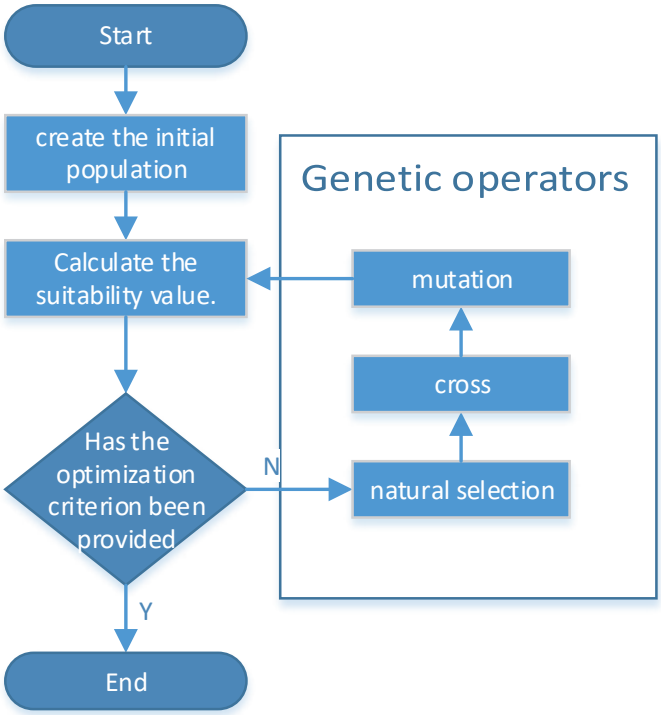

Figure 5. General structure of the genetic algorithm.

CONCLUSION

The speed control issue of DC motors has been examined in this chapter, with an emphasis on the parameter tuning of the popular PID controller. In order to construct its mathematical model, the electrical and mechanical dynamics of an independently stimulated DC motor were taken into consideration when determining the pertinent transfer function for speed control. The PID controller's basic working principles were then explained, along with how the proportional, integral, and derivative terms affected system dynamics.

The methods for determining PID parameters were examined under two main categories: classical tuning techniques and optimization-based approaches. Classical methods despite their simplicity and ease of implementation, may not always provide satisfactory performance for nonlinear systems and varying load conditions. In particular, these methods exhibit limitations in terms of overshoot and settling time performance.

Metaheuristic optimization techniques examined for PID parameter adjustment in order to get beyond these restrictions. Algorithms such as Particle Swarm Optimization, Sine Cosine Algorithm, Whale Optimization Algorithm, Moth–Flame Optimization, Kidney-Inspired Algorithm, Artificial Bee Colony Algorithm, and Genetic Algorithm were briefly described, and their potential to enhance PID controller performance was discussed. Optimization-based tuning approaches are capable of achieving reduced overshoot, shorter settling times, and near-zero steady-state error.

In conclusion, although the PID controller remains a practical and effective solution for DC motor speed control, tuning its parameters using classical methods does not always guarantee optimal performance. By taking into account the nonlinear properties of the system and changing operating conditions, metaheuristic optimization algorithms offer a more adaptable and reliable framework for determining appropriate PID parameters.Therefore, future research may focus on comparative analyses of different optimization techniques, the application of multi-objective optimization strategies, and experimental validation in real-time control environments to further improve DC motor control performance.

REFERENCES

[1] Shekhar, S., Saha, P. K., & Thakura, P. R. (2019, June). Optimal pid tuning of bldc drive using lqr technique. In *2019 IEEE International Conference on Intelligent Systems and Green Technology (ICISGT)* (pp. 57-574). IEEE.

[2] Kumar, P., Chatterjee, S., Shah, D., Saha, U. K., & Chatterjee, S. (2017). On comparison of tuning method of FOPID controller for controlling field controlled DC servo motor. *Cogent Engineering*, *4*(1), 1357875.

[3] Shekhawat, A. S., & Rohilla, Y. (2020, September). Design and control of two-wheeled self-balancing robot using Arduino. In *2020 International Conference on Smart Electronics and Communication (ICOSEC)* (pp. 1025-1030). IEEE.

[4] Chotai, J., & Narwekar, K. (2017, December). Modelling and position control of brushed DC motor. In *2017 international conference on advances in computing, communication and control (ICAC3)* (pp. 1-5). IEEE.

[5] Köse, F., Kaplan, K., & Ertunç, H. M. (2013). PID ve bulanık mantık ile DC motorun gerçek zamanda STM32F407 tabanlı hız kontrolü. *Otomatik Kontrol Ulusal Toplantısı, TOK2013*, 26-28.

[6] Top, A. (2025). Optimization-Based Tuning of PI Controller Parameters for DC Motor Speed Control. *Hittite Journal of Science and Engineering*, *12*(2).

[7] Okoro, I. S., & Enwerem, C. O. (2020). Robust control of a DC motor. *Heliyon*, *6*(12).

[8] Dezaki, M. L., Hatami, S., Zolfagharian, A., & Bodaghi, M. (2022). A pneumatic conveyor robot for color detection and sorting. *Cognitive Robotics*, *2*, 60-72.

[9] Ahmed, M. M., Hassanien, W. S., & Enany, M. A. (2021). Modeling and evaluation of SC MPPT controllers for PVWPS based on DC motor. *Energy Reports*, *7*, 6044-6053.

[10] Hendra, H., Pebriyanto, S., Hernadewita, H., Hermiyetti, H., & Yoserizal, Y. (2021). Applying Programmable Logic Control (PLC) for Control Motors, Blower and Heater in the Rubber Drying Processing. *Jurnal Ilmiah Teknik Elektro Komputer dan Informatika (JITEKI)*, *7*(1), 131-141.

[11] Auzan, M., Hujja, R. M., Fuadin, M. R., & Lelono, D. (2021). Path Tracking and Position Control of Nonholonomic Differential Drive Wheeled Mobile Robot. *Jurnal Ilmiah Teknik Elektro Komputer dan Informatika*, *7*(3), 368-379.

[12] Ashokkumar, R., Suresh, M., Sharmila, B., Panchal, H., Gokul, C., Udhayanatchi, K. V., ... & Israr, M. (2022). A novel method for Arduino based electric vehicle emulator. *International Journal of Ambient Energy*, *43*(1), 4299-4304.

[13] Kocaoğlu S, Kuşçu H. (2012) PIC ile DC motorun hız ve konum kontrolü için gerekli PID parametrelerinin belirlenmesi ve bir uygulama. In: *Otomatik Kontrol Ulusal Toplantısı* (TOK).

[14] Chaouch, S., Hasni, M., Boutaghane, A., Babes, B., Mezaache, M., Slimane, S., & Djenaihi, M. (2018, October). DC-motor control using arduino-uno board for wire-feed system. In *2018 international conference on electrical sciences and technologies in Maghreb (CISTEM)* (pp. 1-6). IEEE.

[15] Găşpăresc, G. (2016, October). PID control of a DC motor using Labview Interface for Embedded Platforms. In *2016 12th IEEE international symposium on electronics and telecommunications (ISETC)* (pp. 145-148). IEEE.

[16] Guo, Y., & Mohamed, M. E. A. (2020). Speed control of direct current motor using ANFIS based hybrid PID configuration controller. *IEEE Access*, *8*, 125638-125647.

[17] Hekimoğlu, B. (2019). Optimal tuning of fractional order PID controller for DC motor speed control via chaotic atom search optimization algorithm. *IEEE access*, *7*, 38100-38114.

[18] Tir, Z., Malik, O., Hamida, M. A., Cherif, H., Bekakra, Y., & Kadrine, A. (2017, October). Implementation of a fuzzy logic speed controller for a permanent magnet dc

motor using a low-cost Arduino platform. In *2017 5th International Conference on Electrical Engineering-Boumerdes (ICEE-B)* (pp. 1-4). IEEE.

[19] Akbar, M. A., Naniwa, T., & Taniai, Y. (2016, August). Model reference adaptive control for DC motor based on Simulink. In *2016 6th International Annual Engineering Seminar (InAES)* (pp. 101-106). IEEE.

[20] Ahmad, M., Khan, A., Raza, M. A., & Ullah, S. (2018, April). A study of state feedback controllers for pole placement. In *2018 5th International Multi-Topic ICT Conference (IMTIC)* (pp. 1-6). IEEE.

[21] Somwanshi, D., Bundele, M., Kumar, G., & Parashar, G. (2019). Comparison of fuzzy-PID and PID controller for speed control of DC motor using LabVIEW. *Procedia Computer Science*, *152*, 252-260.

[28] Joseph, S. B., Dada, E. G., Abidemi, A., Oyewola, D. O., & Khammas, B. M. (2022). Metaheuristic algorithms for PID controller parameters tuning: Review, approaches and open problems. *Heliyon*, *8*(5).

[23] Kherkhar, A., Chiba, Y., Tlemçani, A., & Mamur, H. (2022). Thermal investigation of a thermoelectric cooler based on Arduino and PID control approach. *Case Studies in Thermal Engineering*, *36*, 102249.

[24] Xu, F., Liang, X., Chen, M., & Liu, W. (2022). Robust self-learning PID control of an aircraft anti-skid braking system. *Mathematics*, *10*(8), 1290.

[25] Božek, P., & Nikitin, Y. (2021, August). The development of an optimally-tuned PID control for the actuator of a transport robot. In *Actuators* (Vol. 10, No. 8, p. 195).

[26] Sun, J., Zhou, H., Ma, X., & Ju, Z. (2018). Study on PID tuning strategy based on dynamic stiffness for radial active magnetic bearing. *ISA transactions*, *80*, 458-474.

[27] Alagoz, B. B., Deniz, F. N., & Koseoglu, M. (2022). An efficient PID-based optimizer loop and its application in De Jong's functions minimization and quadratic regression problems. *Systems & Control Letters*, *159*, 105090.

[28] Ulusoy, S., Nigdeli, S. M., & Bekdaş, G. (2021). Novel metaheuristic-based tuning of PID controllers for seismic structures and verification of robustness. *Journal of Building Engineering*, *33*, 101647.

[29] Du, H., Liu, P., Cui, Q., Ma, X., & Wang, H. (2022). PID controller parameter optimized by reformative artificial bee colony algorithm. *Journal of Mathematics*, *2022*(1), 3826702.

[30] Bhookya, J., Kumar, M. V., Kumar, J. R., & Rao, A. S. (2022). Implementation of PID controller for liquid level system using mGWO and integration of IoT application. *Journal of Industrial Information Integration*, *28*, 100368.

[31] Kommula, B. N., & Kota, V. R. (2020). Direct instantaneous torque control of Brushless DC motor using firefly Algorithm based fractional order PID controller. *Journal of King Saud University-Engineering Sciences*, *32*(2), 133-140.

[32] Rodríguez-Molina, A., Villarreal-Cervantes, M. G., Álvarez-Gallegos, J., & Aldape-Pérez, M. (2019). Bio-inspired adaptive control strategy for the highly efficient speed regulation of the DC motor under parametric uncertainty. *Applied Soft Computing*, *75*, 29-45.

[33] Gani, M. M., Islam, M. S., & Ullah, M. A. (2019). Optimal PID tuning for controlling the temperature of electric furnace by genetic algorithm. *SN Applied Sciences*, *1*(8), 880.

[34] Bhookya, J., & Jatoth, R. K. (2019). Optimal FOPID/PID controller parameters tuning for the AVR system based on sine–cosine-algorithm. *Evolutionary Intelligence*, *12*(4), 725-733.

[35] Zhou, Y., Zhang, J., Yang, X., & Ling, Y. (2019). Optimization of PID controller based on water wave optimization for an automatic voltage regulator system. *Information Technology and Control*, *48*(1), 160-171.

[36] Hekimoğlu, B. (2019). Böbrek-ilhamlı algoritma ile ayarlanan PID kontrolör kullanarak DC motor hız kontrolü. *Bitlis Eren Üniversitesi Fen Bilimleri Dergisi*, *8*(2), 652-663.

[37] Şahin, A. K., Akyazı, Ö., Sahın, E., & Çakır, O. (2021). DC Motorun hız kontrolü için meta-sezgisel algoritma tabanlı PID denetleyici tasarımı. *Bitlis Eren Üniversitesi Fen Bilimleri Dergisi*, *10*(2), 533-549.

[38] Kushwah, M., & Patra, A. (2014). Tuning PID controller for speed control of DC motor using soft computing techniques-A review. *Advance in Electronic and Electric Engineering*, *4*(2), 141-148.

[39] Ang, K. H., Chong, G., & Li, Y. (2005). PID control system analysis, design, and technology. *IEEE transactions on control systems technology*, *13*(4), 559-576.

[40] Crenganis, M., & Bologa, O. (2016). Implementing Pid Controller For A Dc Motor Actuated Mini Milling Machine. *Academic Journal of Manufacturing Engineering*, *14*(2).

[41] Farag, W. (2020). Complex trajectory tracking using PID control for autonomous driving. *International Journal of Intelligent Transportation Systems Research*, *18*(2), 356-366.

[42] Türkoğlu, E. C., Tunç, Y., Yaren, T., & Kizir, S. (2023),Pid Parametrelerinin Otomatik Ayarlama Yöntemi İle Kestirimi: Dc Motor Konum Kontrolü. *International Marmara Sciences Congress*

[43] Bansal, H. O., Sharma, R., & Shreeraman, P. R. (2012). PID controller tuning techniques: a review. *Journal of control engineering and technology*, *2*(4), 168-176.

[44] Reis, V. C., Santos, M. F., Carmo, M. J., & Ferreira, F. C. (2016, October). Control of level systems by arduino via PC platform. In *2016 20th International Conference on System Theory, Control and Computing (ICSTCC)* (pp. 251-256). IEEE.

[45] Ziegler, J. G., & Nichols, N. B. (1942). Optimum settings for automatic controllers. *Transactions of the American society of mechanical engineers*, *64*(8), 759-765.

[46] Srinivas, P., Lakshmi, K. V., & Kumar, V. N. (2014). A comparison of PID controller tuning methods for three tank level process. *International Journal of Advanced Research in Electrical, Electronics and Instrumentation Engineering*, *3*(1), 6810-6820.

[47] Gidemen, G., & Furat, M. (2015). PID parametrelerinin ayarlama yöntemleri: 2. derece sistem modeline uygulanması ve karşılaştırmalı olarak değerlendirilmesi.

[48] Raut, K. H., & Vaishnav, S. R. (2014). Performance analysis of PID tuning techniques based on time response specification. *International Journal of Innovative Research in Electrical, Electronics, Instrumentation and Control Engineering*, *2*(1), 616-619.

[49] Bandyopadhyay, S., Chakraborty, R., & Maulik, U. (2015). Priority based∈ dominance: A new measure in multiobjective optimization. *Information Sciences*, *305*, 97-109.

[50] Uygur, A. F. (2025). Ayrişima Dayali Çok Amaçli Evrimsel Algoritma Üzerinden Pid Kontrolcü Parametrelerinin Optimizasyonu. *Kahramanmaraş Sütçü İmam Üniversitesi Mühendislik Bilimleri Dergisi*, *28*(3), 1143-1158.

[51] Joseph, S. B., Dada, E. G., Abidemi, A., Oyewola, D. O., & Khammas, B. M. (2022). Metaheuristic algorithms for PID controller parameters tuning: Review, approaches and open problems. *Heliyon*, *8*(5).

[52] Eberhart, R., & Kennedy, J. (1995, October). A new optimizer using particle swarm theory. In *MHS'95. Proceedings of the sixth international symposium on micro machine and human science* (pp. 39-43).

[53] Garip, Z., Karayel, D., & Çimen, M. E. (2021). Parçacık Sürü Optimizasyon Tabanlı Mobil Robotlarda Global Yol Planlama. *Journal of Smart Systems Research*, *2*(1), 18-26.

[54] Ekinci, S., Hekimoğlu, B., Demirören, A., & Eker, E. (2019, October). Speed control of DC motor using improved sine cosine algorithm based PID controller. In *2019 3rd*

International Symposium on Multidisciplinary Studies and Innovative Technologies (ISMSIT) (pp. 1-7). IEEE.

[55] Wu, C., Chen, L., Xiong, H., & Hu, J. (2024). USMN-SCA: A Blockchain Sharding Consensus Algorithm With Tolerance for an Unlimited Scale of Malicious Nodes. *IEEE Transactions on Network and Service Management*.

[56] Nadimi-Shahraki, M. H., Taghian, S., Javaheri, D., Sadiq, A. S., Khodadadi, N., & Mirjalili, S. (2024). MTV-SCA: multi-trial vector-based sine cosine algorithm. *Cluster Computing*, *27*(10), 13471-13515.

[57] Yousef, A. M., Ebeed, M., Abo-Elyousr, F. K., Elnozohy, A., Mohamed, M., & Abdelwahab, S. M. (2020). Optimization of PID controller for hybrid renewable energy system using adaptive sine cosine algorithm. *International Journal of Renewable Energy Research-IJRER*, 670-677.

[58] Nanyan, N. F., Ahmad, M. A., & Hekimoğlu, B. (2024). Optimal PID controller for the DC-DC buck converter using the improved sine cosine algorithm. *Results in Control and Optimization*, *14*, 100352.

[59] Mirjalili, S., & Lewis, A. (2016). The whale optimization algorithm. *Advances in engineering software*, *95*, 51-67.

[60] Mirjalili, S. (2015). Moth-flame optimization algorithm: A novel nature-inspired heuristic paradigm. *Knowledge-based systems*, *89*, 228-249.

[61] Hekimoğlu, B. (2019). Böbrek-ilhamlı algoritma ile ayarlanan PID kontrolör kullanarak DC motor hız kontrolü. *Bitlis Eren Üniversitesi Fen Bilimleri Dergisi*, *8*(2), 652-663.

[62] Jaddi, N. S., Alvankarian, J., & Abdullah, S. (2017). Kidney-inspired algorithm for optimization problems. *Communications in Nonlinear Science and Numerical Simulation*, *42*, 358-369.

[63] Jaddi, N. S., & Abdullah, S. (2018). Optimization of neural network using kidney-inspired algorithm with control of filtration rate and chaotic map for real-world rainfall forecasting. *Engineering Applications of Artificial Intelligence*, *67*, 246-259.

[64] Pham, D. T., Ghanbarzadeh, A., Koç, E., Otri, S., Rahim, S., & Zaidi, M. (2006). The bees algorithm—a novel tool for complex optimisation problems. In *Intelligent production machines and systems* (pp. 454-459). Elsevier Science Ltd.

[65] Tarhan, A., & Kalyoncu, M. (2024). Design Of Optimal Pid Controller For A Dc Motor Using The Bees Algorithm. *11. International European Congress On Advanced Studies In Basic Sciences*

[66] Goldberg, D., Holland, J. (1988). Genetic Algorithms and Machine Learning. *Mach. Learn.*, 3(2-3): 95–99.

[67] Erkol, H. O. (2017). GA ve PSO ile Kontrol Parametrelerinin Optimizasyonu. *Karaelmas Fen ve Mühendislik Dergisi*, *7*(1), 179-185.